AN INVERSE ADVECTIVE MODEL OF THE OCEAN MIXED LAYER FOR PALEOCEANOGRAPHIC STUDIES: MANUAL OF COMPUTER CODE

Version V1

Olivier Marchal

Woods Hole Oceanographic Institution
Woods Hole, MA 02543, USA
Tel: +1 508 289 3374
Fax: +1 508 457 2187
email: omarchal@whoi.edu

September 29, 2015

Contents

1 Foreword **5**

2 Introduction **6**

3 Disclaimer **8**

4 Time-Dependent Inverse Problem **9**

4.1 Sediment SST Records 9

4.1.1 Sediment Core Chronologies 9

4.1.2 SST Reconstructions 10

4.2 Advective Model of Ocean Mixed Layer 10

4.2.1 Equations of Motion 11

4.2.2 Equation for Mixed Layer Temperature 12

4.2.3 Horizontal Velocity $\bar{\mathbf{u}}$ 14

4.2.4 Vertical Velocity w_I and w_A 15

4.2.5 Model Domain and Boundary Conditions 16

4.2.6 Method of Solution 17

4.2.7 Solution for the Modern North Atlantic 19

4.3 Sequential Methods 21

4.3.1 State Vector 21

4.3.2 Observation and Dynamic Equations 22

4.3.3 Observation and Model Errors 23

4.3.4 Kalman Filters 25

4.3.5 Linearized Smoother 28

4.4 Examples of Filtered and Smoothed Solutions 31

4.4.1 LKF Solution 31

4.4.2 Comparing EKF and LKF Solutions 33

4.4.3 Smoothed Solution 33

5 Computer Code **35**

5.1 Main Program 35

5.2 Routines 37

5.2.1 *coepoly.f* 37

5.2.2 *df-dxxx.f* 38

5.2.3 *EExxxxx.f* 39

5.2.4 *fil-ekf.f* 39

5.2.5 *fil-lkf.f* 39

5.2.6 *freezin.f* 40

5.2.7 *iaxxxxx.f* 40

5.2.8 *mod-int.f* 40

5.2.9 *mod-sta.f* 41

5.2.10 *num-rec.f* 41

5.2.11 *opening.f* 41

5.2.12 *P-filxx.f* 42

5.2.13 *QQxxxxx.f* 42

5.2.14 *reading.f* 43

5.2.15 *selxxxx.f* 43

5.2.16 *setting.f* 44

5.2.17 *smoothe.f* 44

5.2.18 *stringx.f* 44

5.2.19 *sv-to-x.f* 44

5.2.20 *uuxxxxx* 45

5.2.21 *vvxxxxx* 45

5.2.22 *w-ixxxx.f* 45

5.2.23 *writing.f* 45

5.2.24 *wr-xfil.f* . . . 46

5.2.25 *wr-xmxx.f* . . . 46

5.2.26 *x-to-sv.f* . . . 46

5.2.27 *zzRRHob.f* . . . 47

5.3 Common File . . . 48

5.4 Makefile . . . 49

6 Preparing an Inversion & Running the Program **50**

6.1 Preparing an Inversion . . . 50

6.2 Running the Program . . . 53

7 Acknowledgements **54**

8 Appendices **55**

8.1 Appendix A: Modern Observational Estimates of $T_A, T_I, S, h, \boldsymbol{\tau}_s$ . . . 55

8.2 Appendix B: Estimation of Polynomial Coefficients . . . 56

8.3 Appendix C: Matrix of partial derivatives $\partial \mathbf{f}/\partial \mathbf{x}$ . . . 57

9 References **63**

10 Tables **68**

10.1 Table 1: Parameters of the Ocean Mixed Layer Model . . . 68

10.2 Table 2: Integral exponents of the polynomial approximations . . . 68

11 Figures **69**

1 Foreword

A FORTRAN code has been developed to combine long records of sea surface temperature (SST) generated in paleoceanography with an advective model of the ocean mixed layer using sequential methods. The sequential methods are a linearized Kalman filter, an extended Kalman filter, and a linearized smoother. The code as presently written represents an application of these methods to a region of the North Atlantic. It has been used to infer an evolution of SST in this region over the past 14,500 yr which is consistent in the least-squares sense with both the data records and the model physics, given estimates of their respective error (co)variances. It can be run with modest computational resources and should be applicable to solve time-dependent inverse problems of a similar nature with relatively small programing effort.

2 Introduction

The interpretation of data records from sediments, corals, etc., in terms of past ocean states is a major but challenging task of paleoceanography. The records suffer generally from significant uncertainties, have poor spatial and temporal resolutions (by modern instrumental standards), and are sometimes inconsistent. An ocean model provides a dynamical approach to interpolating or extrapolating inaccurate, sparse, and inconsistent data. By considering ocean dynamics, the analysis of such data may produce more reliable ocean state estimates, particularly in places where, and at times when, no data exist.

In broadest terms, inverse methods constitute a body of techniques that can be used to combine observations with a model (*Wunsch*, 2006). Different inverse methods are available to combine data records with a dynamical model, such as adjoint methods based on Lagrange multipliers and sequential methods of optimal estimation theory. In both cases, the estimation of the uncertainty in the inferred time-dependent states is an issue: for adjoint methods it is in general not part of the solution, whereas for sequential methods it may overwhelm the computation. Given their high computational load, sequential methods have been rarely applied to oceanography and paleoceanography, in spite of the strong desirability for error estimates in these fields of research (for a review, see *Edwards et al.*, 2015).

In this document, we describe a computer code for the application of sequential methods to combine long records of sea surface temperature (SST) that are generated in the field of paleoceanography with a simplified advective model of the ocean mixed layer. The temporal evolution of the surface ocean state over the data span is estimated from the combination of the SST records with the model using a Kalman filter and a related smoother. These methods offer two main advantages in the present context. First, they permit the inference of a time-evolving ocean state that is consistent (in the least-squares sense) with both the data records and the model physics, given estimates of their respective error (co)variances. Second, they provide estimates of the uncertainties in the time-evolving states through a formal propagation of the estimated errors in the data and in

the model. As a result, the significance of the inferred changes in the oceanic fields can be evaluated.

This document is organized as follows. In section 2, we describe the time-dependent inverse problem as it is currently implemented and solved in the code. The data records, the model equations, and the sequential methods used to combine the data with the model are presented in turn. A set of figures are included and commented which illustrate an application of these methods to the inference of the time-dependent state of the ocean mixed in a North Atlantic region over the past 14,500 yr. In section 3, the computer code is presented. We describe its major entities as well as the main tasks completed by them. Finally, in section 4, the set of operations that are required in order to run the code is listed.

3 Disclaimer

Although the present computer code is only intermediate in size and has been subject to repeated tests, no claim is made that it is error-free. The author would welcome notifications of inconsistencies, obscurities, and (or) errors in the present program and (or) the present document. Nor it is claimed that the operations being carried out have been programed with maximum efficiency. In fact, as the user will probably notice, efficiency in programing has largely been sacrificed for code legibility. It is hoped that this approach will help the user to better understand the code and to apply it for his or her own investigation. Finally, no effort has been made to produce a code with maximum flexibility, although many aspects of the program have been developed with an eye toward its applications to other research problems.

4 Time-Dependent Inverse Problem

In this section, we describe the time-dependent inverse problem that is implemented and solved in the computer code. Broadly, the problem consists in producing an estimate of the time-dependent state of the surface North Atlantic over the past 14,500 yrs, a time interval characterized by climatic changes, by combining three SST records with an advective ocean mixed-layer model using sequential methods.

4.1 Sediment SST Records

The records of SST that are currently considered in the code have been generated from sediment cores raised from three locations in the North Atlantic (Fig. 1): core SU81-18 from the western Iberian margin (37°46'N, 10°11'W, water depth 3,135 m), core CH69-K09 from the Newfoundland Basin (41°45'N, 47°21'W, 4,100 m), and core NA87-22 from the Rockall Trough (55°29'N, 14°41'W, 2,161 m).

4.1.1 Sediment Core Chronologies

The chronologies of the three records have been established from ^{14}C dates measured on monospecific planktonic foraminifera (*Bard et al.*, 1987; *Duplessy et al.*, 1992; *Labeyrie et al.*, 1999). The number of planktonic foraminiferal ^{14}C dates amounts to 30 for core SU81-18, 13 for core CH69-K09, and 25 for core NA87-22. Radiocarbon ages were converted into calendar age estimates using (i) the CALIB 4.1 software (*Stuiver and Reimer*, 1993), (ii) the 310-yr moving average marine calibration curve of *Stuiver et al.* (1998), and (iii) reservoir ages constrained from the assumption that the two deglacial warming events apparent in each record were synchronous with the onset of the Bølling (14.53±0.53 kyr BP) and the end of the Younger Dryas (YD, 11.60 ± 0.25 kyr BP) in the GRIP ice core, Central Greenland (dates from *Waelbroeck et al.*, 2001). Further details about the sediment core chronologies can be found in this paper.

4.1.2 SST Reconstructions

Estimates of sea surface temperature were derived for each of the three sediment cores from planktonic foraminiferal counts (*Waelbroeck et al.*, 2001). The faunal counts were converted into SST estimates for the 'cold' and 'warm' seasons using the revised analog method (RAM) developed by *Waelbroeck et al.* (1998). The SST records used in the code are produced by averaging the cold and warm season SSTs for each of the three cores (Fig. 2). The uncertainties in the averaged SSTs are calculated by propagating the errors in the seasonal values, assuming no error correlation. The number of SST estimates for the past 14.5 kyr BP is equal to 24 for core SU81-18, 103 for core CH69-K09, and 96 for core NA87-22. These values imply a mean temporal resolution of, respectively, 604 yr, 141 yr, and 151 yr for these cores.

The SST records derived from the three sediment cores show noticeable temporal variations during the last deglaciation (Fig. 2). Common to all three records are the occurrences of relatively (i) high SSTs during the Bølling-Allerød (ca. 14.7 to 13.0 kyr BP), (ii) low SSTs during the YD (ca. 13.0 to 11.6 kyr BP), and (iii) high SSTs during the Holocene (ca. 11.6 to 0 kyr BP), which in part reflects the common chronological assumptions for the records.

4.2 Advective Model of Ocean Mixed Layer

In this section, we describe the ocean model that is used in order to constrain, in concert with the SST records, the time-dependent state of the surface North Atlantic over the past 14.5 kyrs. Early models of the ocean mixed layer (ML) were developed primarily to study diurnal and seasonal variations in the upper ocean (e.g., *Kraus and Turner*, 1967; *Niiler and Krauss*, 1977; *Price et al.*, 1986). These models assume that properties such as temperature and salinity are vertically uniform in the layer and neglect the effects of horizontal transport in the equations of motion. In spite of these limitations, these one-dimensional bulk models can reproduce changes in surface temperature and ML depth which have been observed at open-open stations (e.g., *Martin*, 1985; *Gaspar*, 1988).

Horizontal advection, however, may significantly influence the ML heat balance on longer time scales (*Gill and Niiler*, 1973) or in regions of strong horizontal gradients (e.g., *Rudnick and Weller*, 1993). Efforts to incorporate horizontal advection in bulk models of the ML were undertaken in the 1980s (e.g., *de Szoeke*, 1980; *Welander*, 1981; *Cushman-Roisin*, 1981; *de Ruijter*, 1983b; *de Ruijter*, 1983a; *Rudnick and Davis*, 1988). These studies illustrated, for example, that Ekman convergence can develop a thermal front in the ML, even in the presence of a constant horizontal gradient of atmospheric temperature (e.g., *Welander*, 1981).

The model being coded is an advective bulk model of the ML, where temperature and salinity are vertically uniform in the layer but where the effect of horizontal advection is retained (Fig. 3). The ML extends from the sea surface at $z = 0$ to the base of the mixed layer at $z = -h$. Below the ML is a transition zone with a thickness δ and characterized by a relatively strong vertical density gradient. The transition zone separates the strongly turbulent ML above from the weakly turbulent stratified interior below. A transition zone is often postulated in bulk models of the ML (e.g., *Niiler and Krauss*, 1977) and has been the focus of recent observational studies (e.g., *Johnston and Rudnick*, 2009; *Sun et al.*, 2013). In our model, the transition zone is assumed to be thin compared to the ML, i.e., $\delta \ll h$. Moreover, the horizontal motion at the base of the transition zone is taken to be small relative to that in the ML, as in previous models (e.g., *de Szoeke*, 1980; *Welander*, 1981; *Cushman-Roisin*, 1981).

4.2.1 Equations of Motion

Our ML model is based on the following set of dynamical equations: an approximate balance for horizontal momentum, the hydrostatic approximation, the statement of volume conservation, governing equations for temperature and salinity, and an equation of state. Respectively,

$$f\hat{\mathbf{z}} \times \mathbf{u} = -\frac{1}{\rho_o}\nabla p + \frac{1}{\rho_o}\frac{\partial \boldsymbol{\tau}}{\partial z}, \tag{1a}$$

$$0 = -\frac{1}{\rho}\frac{\partial p}{\partial z} - g, \tag{1b}$$

$$\nabla \cdot \mathbf{u} + \frac{\partial w}{\partial z} = 0, \tag{1c}$$

$$\frac{\partial T}{\partial t} + \nabla \cdot (\mathbf{u}T) + \frac{\partial}{\partial z}(wT) = \frac{\partial q_T}{\partial z}, \tag{1d}$$

$$\frac{\partial S}{\partial t} + \nabla \cdot (\mathbf{u}S) + \frac{\partial}{\partial z}(wS) = \frac{\partial q_S}{\partial z}, \tag{1e}$$

where

$$\rho = \rho_o - \rho_o \alpha (T - T_o) + \rho_o \beta (S - S_o). \tag{2}$$

The dynamical variables in (1a–1d) are the horizontal velocity $\mathbf{u}$, the vertical velocity component w, the pressure p, the density ρ, the temperature T, and the salinity S. Other quantities in (1a–1d) include the Coriolis parameter $f = 2\Omega \sin\phi$, where Ω is the Earth angular velocity and ϕ is latitude, a reference density ρ_o, temperature T_o, and salinity S_o, the acceleration due to gravity g, the horizontal stress $\boldsymbol{\tau}$, the vertical temperature (salinity) flux q_T (q_S), the thermal expansion coefficient α, and the haline contraction coefficient β. Finally, ∇ is the horizontal gradient operator, $\hat{\mathbf{z}}$ is a unit vector pointing upwards, and t is time.

It is probably worth being explicit about the major dynamical assumptions in (1). Equation (1a) represents a balance between the Coriolis acceleration, the pressure gradient force, and the frictional force caused by the vertical divergence of a horizontal stress. This balance is thought to constitute a valid approximation for the large-scale flow in the oceanic interior but not near western boundaries, for example, where horizontal friction and inertia should be important (*Pedlosky*, 1996). The temperature and salinity equations (1d–1e) account for the effects of local storage, horizontal transport by the large-scale flow, and vertical divergences. They omit the effects of horizontal transport by small-scale phenomena (eddies), which could be important, for example, for the Subpolar Front near the Middle Atlantic Ridge (e.g., *Arhan et al.*, 1989; *Colin de Verdière et al.*, 1989; *Read et al.*, 2010).

4.2.2 Equation for Mixed Layer Temperature

The equation for ML temperature is the governing equation of our model. It is derived as follows (e.g., *Welander*, 1981). Since $\delta \ll h$, the vertical integral of equation (1d) from

$z = -(h+\delta)$ to $z = 0$ yields

$$h\frac{\partial T}{\partial t} + \nabla \cdot (h\bar{\mathbf{u}}T) - (\mathbf{u}T)\,|_{-(h+\delta)} \cdot \nabla h - (wT)|_{-(h+\delta)} = q|_0 - q|_{-(h+\delta)}, \tag{3}$$

upon application for the Leibniz rule for the differentiation of an integral with variable limits and assuming that the vertical velocity at the sea surface vanishes. Here $\bar{\mathbf{u}}$ is the vertical average of the horizontal velocity in the ML,

$$\bar{\mathbf{u}} = \frac{1}{h}\int_{-h}^{0} \mathbf{u}dz, \tag{4}$$

i.e., the small contribution due to transport in the layer of thickness δ has been neglected.

Horizontal advection influences the ML heat balance through the second and third terms on the left-hand side of (3). The second term, $\nabla \cdot (h\bar{\mathbf{u}}T)$, represents the horizontal heat divergence caused by the mean flow. Its order of magnitude is $O(HUT_*/L)$, where (H, U, T_*, L) are characteristic values for, respectively, the ML depth, the ML horizontal velocity, the ML temperature, and the horizontal scale of variation of $h\bar{\mathbf{u}}T$. The third term, $(\mathbf{u}T)\,|_{-(h+\delta)} \cdot \nabla h$, describes the effect of the horizontal heat flux at the base of the transition zone along the gradient of ML depth. Its order of magnitude is $O(U_i T H/L_h)$, where (U_i, L_h) are characteristic values for, respectively, the horizontal velocity at $z = -(h+\delta)$ and the horizontal scale of variation of h. Thus, the ratio of the third term to the second term is $O((U_i/U)L/L_h)$. From our assumption that $U_i/U \ll 1$ and provided that L_h is on the same order as (or greater than) L, the term $(\mathbf{u}T)\,|_{-(h+\delta)} \cdot \nabla h$ is taken to be small compared to $\nabla \cdot (h\bar{\mathbf{u}}T)$. As a result, the heat balance equation (3) reduces to

$$h\frac{\partial T}{\partial t} + \nabla \cdot (h\bar{\mathbf{u}}T) - (wT)|_{-(h+\delta)} = w_A\,(T_A - T)\,. \tag{5}$$

Here the temperature flux near the base of the ML, $q|_{-(h+\delta)}$ has been assumed to be small compared to that at the surface, $q|_0$, and $q|_0$ has been represented as a Newtonian cooling, where T_A is an apparent atmospheric temperature and w_A is a parameter that describes the strength of heat exchange between the atmosphere and the ML (*Welander*, 1981; *de Ruijter*, 1983b).

The precise form of the ML temperature equation is obtained as follows. The vertical

velocity $w_{-(h+\delta)}$ in (5) is derived from the integration of (1c) from $z = -(h+\delta)$ to $z = 0$,

$$w_{-(h+\delta)} = \nabla \cdot (h\bar{\mathbf{u}})\,. \tag{6}$$

Here the term $\mathbf{u}|_{-(h+\delta)} \cdot \nabla h$, which is $\mathrm{O}(U_i H/L_h)$, has been taken as negligible compared to $\nabla \cdot (h\bar{\mathbf{u}})$, which is $\mathrm{O}(UH/L_h)$, consistent with our scaling assumptions. The insertion of (6) into (5) leads finally to

$$\frac{\partial T}{\partial t} + \bar{\mathbf{u}} \cdot \nabla T = \frac{w_I}{h}\,(T_I - T) + \frac{w_A}{h}\,(T_A - T)\,, \tag{7}$$

where $w_I \equiv w_{-(h+\delta)}$ is the interior vertical velocity and $T_I \equiv T_{-(h+\delta)}$ is the interior temperature. Equation (7) is the equation for ML temperature in our model. According to (7), warming or cooling in the ML is caused by horizontal heat advection by the mean flow, heat exchange with water from below the ML, and (or) heat exchange with the atmosphere. A similar balance has been used to interpret SST variability on interannual and longer time scales over the span of instrumental records (e.g., *Deser et al.*, 2010).

4.2.3 Horizontal Velocity $\bar{\mathbf{u}}$

The horizontal velocity, $\bar{\mathbf{u}}$, in (7) is derived from the momentum equations (1a–1b). Since (1a) is linear in $\mathbf{u}$, the velocity $\mathbf{u}$ can be taken as the sum of an Ekman velocity, $\mathbf{u}_e$, and a geostrophic velocity, $\mathbf{u}_g$, i.e., $\mathbf{u} = \mathbf{u}_e + \mathbf{u}_g$, where

$$f\hat{\mathbf{z}} \times \mathbf{u}_e = \frac{1}{\rho_o}\frac{\partial \boldsymbol{\tau}}{\partial z} \qquad \text{and} \qquad f\hat{\mathbf{z}} \times \mathbf{u}_g = -\frac{1}{\rho_o}\nabla p. \tag{8}$$

Clearly, $\bar{\mathbf{u}} = \bar{\mathbf{u}}_e + \bar{\mathbf{u}}_g$. Consider first $\bar{\mathbf{u}}_e$, the vertical average of the Ekman velocity in the ML. This is easily obtained by integrating the first equation in (8) from $z = -(h+\delta)$ to $z = 0$, which leads to

$$\bar{\mathbf{u}}_e = \frac{\boldsymbol{\tau}_s \times \hat{\mathbf{z}}}{\rho_o h f}. \tag{9}$$

Here $\boldsymbol{\tau}_s$ is the surface wind stress and the stress at the bottom of the transition zone has been assumed to be negligible.

Consider then $\bar{\mathbf{u}}_g$, the vertical average of the geostrophic velocity in the ML. The second equation in (8) is differentiated with respect to depth, which yields, using the hydrostatic

approximation (1b) and the equation of state (2),

$$\frac{\partial \mathbf{u}_g}{\partial z} = \frac{g}{f}\hat{\mathbf{z}} \times (\alpha \nabla T - \beta \nabla S)\,. \tag{10}$$

The vertical shear of the geostrophic velocity is uniform in the ML, since both temperature and salinity are uniform in the layer. Thus, the geostrophic velocity varies linearly with depth in the ML, which can be written as

$$\mathbf{u}_g(z) = \mathbf{u}_g|_{-(h+\delta)} + \frac{\partial \mathbf{u}_g}{\partial z}\,(z+h)\,, \tag{11}$$

since $\delta \ll h$. Averaging this equation from $z = -(h+\delta)$ to $z = 0$ yields, using (10),

$$\bar{\mathbf{u}}_g = \frac{gh}{2f}\hat{\mathbf{z}} \times (\alpha \nabla T - \beta \nabla S)\,. \tag{12}$$

Here the interior geostrophic velocity, $\mathbf{u}_g|_{-(h+\delta)}$, has been assumed to be small compared to the average geostrophic velocity in the ML, $\bar{\mathbf{u}}_g$, consistent with our scaling assumptions.

Note that, under the approximations above, the thermal contribution to the geostrophic flow,

$$\bar{\mathbf{u}}_T = \frac{\alpha g h}{2f}\hat{\mathbf{z}} \times \nabla T, \tag{13}$$

does not transport heat, since the scalar product of this vector with the temperature gradient ∇T vanishes identically. As a result, heat is carried horizontally in the model only by the Ekman flow, $\bar{\mathbf{u}}_e$, and by the saline contribution to the geostrophic flow,

$$\bar{\mathbf{u}}_S = -\frac{\beta g h}{2f}\hat{\mathbf{z}} \times \nabla S. \tag{14}$$

4.2.4 Vertical Velocity w_I and w_A

The equation for ML temperature (7) includes, in addition to the effect of horizontal advection, the heat exchange with water from below the ML and the heat exchange with the atmosphere. The first term depends on the interior vertical velocity w_I, whereas the second depends on w_A. Consider first w_I. From equation (6) and given the different contributions to the horizontal velocity in the ML,

$$w_I = \nabla \cdot \left(h\left[\bar{\mathbf{u}}_e + \bar{\mathbf{u}}_T + \bar{\mathbf{u}}_S\right]\right). \tag{15}$$

The vertical velocity near the base of the ML, w_I, is equal to the divergence of the total horizontal transport in the ML.

Consider then w_A. *Haney* (1971) proposed, as a surface thermal boundary condition for ocean circulation models, that the surface heat flux be set equal to $Q_2(T_A - T)$, where Q_2 is a parameter with units of W m^{-2} °C^{-1}. Based on zonal and time averaged quantities, this author reported observational estimates of Q_2 in the range from about 25 W m^{-2} °C^{-1} to about 50 W m^{-2} °C^{-1}. The parameter $w_A = Q_2/(\rho_o C_p)$ would therefore vary between 6×10^{-6} and 12×10^{-6} m s^{-1}, considering a density $\rho_o = 1025$ kg m^{-3} and a heat capacity at constant pressure $C_p = 4000$ J kg^{-1} °C^{-1} for seawater.

4.2.5 Model Domain and Boundary Conditions

The domain of the ML model is a region between 36°–62°N and 11°–47°W in the North Atlantic (Fig. 1). It is surrounded by open boundaries. A number of open boundary conditions have been devised for use with regional ocean models (for a review see, e.g., *Marchesiello et al.*, 2001). In general, since the variables at open boundaries would be determined by the equations of motion if the model boundary were extended, it seems sensible to use these equations, or at least their dominant terms, in order to determine variables at open boundaries (*Stevens*, 1990). In this spirit, temperature at the open boundaries of our domain is assumed to be governed solely by the heat exchange with the atmosphere,

$$\frac{\partial T}{\partial t} = \frac{w_A}{h}\,(T_A - T)\,. \tag{16}$$

With this open boundary condition, the temperature evolution at the open boundaries would follow approximately that in the interior of the domain, provided that surface heat exchange is a leading-order term in the ML temperature equation. A test of this condition is provided in section 4.2.7.

4.2.6 Method of Solution

The mixed-layer model consists of the governing equation for temperature (7), together with the expressions for (i) the Ekman velocity (9), (ii) the geostrophic velocity (12) with its thermal (13) and saline contributions (14), and (iii) the interior velocity w_I (15). The (open) boundary condition is provided by (16). The model is solved numerically using a finite-difference method and spherical coordinates. The temporal and spatial derivatives in (7) and (13–16) are approximated with finite differences derived for a staggered grid with uniform longitude and latitude spacings $\Delta\lambda = \Delta\phi = 2^\circ$ (Fig. 1). A time step $\Delta t = 0.1$ yr is used for the model integrations, unless stipulated otherwise.

The grid of the numerical model is arranged as follows (Fig. 4). To lighten notation, the bar over the velocities, which is used to denote vertical averages, is omitted or used for another purpose in this section. The zonal (meridional) component of $\mathbf{u}_* = (\mathbf{u}_e + \mathbf{u}_s)$ is noted by u_* (v_*) and the zonal (meridional) component of surface wind stress is designated by $\tau^{(\lambda)}$ ($\tau^{(\phi)}$). The values of (T, T_A, T_I, S, h) are carried by grid points at the center of the $2^\circ \times 2^\circ$ cells. The values of (u_*, u_e, u_T, u_S) are carried by points along the meridional boundaries of the cells, at the same latitudes as the (T, T_A, T_I, S, h)-carrier points but halfway between these points. Likewise, the values of (v_*, v_e, v_T, v_S) are carried by points along the zonal boundaries of the cells, at the same longitudes as the (T, T_A, T_I, S, h)-carrier points but halfway between these points. Note that the open boundaries include only (T, T_A, T_I, S, h)-carrier points. The horizontal velocity components are all defined at grid points inside the domain, so that no condition on the horizontal flow is needed at the open boundaries.

With this arrangement of the grid, the finite-difference approximations of (7) and (13–16) are as follows. In this section, i is a longitude index, j a latitude index, and n a time index. Consider first (7), the equation for ML temperature. The advection term, $\mathbf{u}_* \cdot \nabla T = \nabla \cdot (\mathbf{u}_* T) - T \nabla \cdot \mathbf{u}_*$, is expressed as

$$\mathbf{u}_* \cdot \nabla T = \mathcal{A}_1 - \mathcal{A}_2, \tag{17}$$

where

$$\mathcal{A}_1 = \frac{1}{r\cos\phi}\frac{\partial uT}{\partial\lambda} + \frac{1}{r}\frac{\partial vT}{\partial\phi}, \tag{18a}$$

$$\mathcal{A}_2 = T\left(\frac{1}{r\cos\phi}\frac{\partial u}{\partial\lambda} + \frac{1}{r}\frac{\partial v}{\partial\phi}\right), \tag{18b}$$

since the term $-(vT/r)\tan\phi$ vanishes in the difference $\nabla\cdot(\mathbf{u}_* T) - T\nabla\cdot\mathbf{u}_*$. Equation (7) is then discretized using an upstream advection scheme,

$$\frac{T^{n+1}_{\mathrm{i,j}} - T^n_{\mathrm{i,j}}}{\Delta t} + \mathcal{D}\left(\mathcal{A}_1\right)^n_{\mathrm{i,j}} - \mathcal{D}\left(\mathcal{A}_2\right)^n_{\mathrm{i,j}} = \dot{T}^n_{\mathrm{i,j}}, \tag{19}$$

where

$$\mathcal{D}\left(\mathcal{A}_1\right)^n_{\mathrm{i,j}} = \frac{(u_*T)^n_{\mathrm{i+1/2,j}} - (u_*T)^n_{\mathrm{i\text{-}1/2,j}}}{r\cos\phi_j\Delta\lambda} + \frac{(v_{*,c}T)^n_{\mathrm{i,j+1/2}} - (v_{*,c}T)^n_{\mathrm{i,j\text{-}1/2}}}{r\Delta\phi}, \tag{20a}$$

$$\mathcal{D}\left(\mathcal{A}_2\right)^n_{\mathrm{i,j}} = T^n_{\mathrm{i,j}}\left(\frac{u^n_{*,\mathrm{i+1/2,j}} - u^n_{*,\mathrm{i\text{-}1/2,j}}}{r\cos\phi_j\Delta\lambda} + \frac{(v_{*,c})^n_{\mathrm{i,j+1/2}} - (v_{*,c})^n_{\mathrm{i,j\text{-}1/2}}}{r\Delta\phi}\right) \tag{20b}$$

and

$$\dot{T}^n_{\mathrm{i,j}} = \frac{w_A}{h^n_{\mathrm{i,j}}}\left(T^n_{A,\mathrm{i,j}} - T^n_{\mathrm{i,j}}\right) + \frac{w^n_{I,\mathrm{i,j}}}{h^n_{\mathrm{i,j}}}\left(T^n_{I,\mathrm{i,j}} - T^n_{\mathrm{i,j}}\right). \tag{21}$$

In (20a–20b), $v_{*,c}$ stands for $v_*\cos\phi$ and r is the Earth radius. The advective fluxes in (20a–20b) are evaluated at locations halfway between the T-carrier points:

$$(u_*T)_{\mathrm{i+1/2,j}} = \frac{1}{2}\left(u_{*,\mathrm{i+1/2,j}} + |u_{*,\mathrm{i+1/2,j}}|\right)T_{\mathrm{i,j}} + \frac{1}{2}\left(u_{*,\mathrm{i+1/2,j}} - |u_{*,\mathrm{i+1/2,j}}|\right)T_{\mathrm{i+1,j}}, \tag{22a}$$

$$(u_*T)_{\mathrm{i\text{-}1/2,j}} = \frac{1}{2}\left(u_{*,\mathrm{i\text{-}1/2,j}} + |u_{*,\mathrm{i\text{-}1/2,j}}|\right)T_{\mathrm{i\text{-}1,j}} + \frac{1}{2}\left(u_{*,\mathrm{i\text{-}1/2,j}} - |u_{*,\mathrm{i\text{-}1/2,j}}|\right)T_{\mathrm{i,j}}. \tag{22b}$$

Similar equations are used for $(v_{*,c}T)_{\mathrm{i,j}\pm1/2}$. Note that in (22) all the variables are implicitly defined at the time level n. The same convention is adopted below, unless specified otherwise.

Consider then (9), the Ekman velocity in the mixed layer. The Ekman velocity components are obtained from

$$u_{e,\mathrm{i+1/2,j}} = \frac{\tau_{\phi,\mathrm{i+1/2,j}}}{\rho_o f_j \bar{h}_{\mathrm{i+1/2,j}}}, \qquad v_{e,\mathrm{i,j+1/2}} = -\frac{\tau_{\lambda,\mathrm{i,j+1/2}}}{\rho_o f_{\mathrm{j+1/2}} \bar{h}_{\mathrm{i,j+1/2}}}. \tag{23}$$

where τ_λ (τ_ϕ) is the zonal (meridional) wind stress component.

Consider (13), the thermal contribution to the geostrophic velocity. The zonal and meridional components of this contribution are computed from, respectively,

$$(u_T)_{\mathrm{i+1/2,j}} = \frac{\alpha g \bar{h}_{\mathrm{i+1/2,j}}}{4r\Omega} \frac{\bar{T}_{\mathrm{i+1/2,j+1}} - \bar{T}_{\mathrm{i+1/2,j\text{-}1}}}{\cos\phi_{\mathrm{j+1}} - \cos\phi_{\mathrm{j\text{-}1}}}, \tag{24a}$$

$$(v_T)_{\mathrm{i,j+1/2}} = \frac{\alpha g \bar{h}_{\mathrm{i,j+1/2}}}{4r\Omega} \frac{\bar{T}_{\mathrm{i+1,j+1/2}} - \bar{T}_{\mathrm{i\text{-}1,j+1/2}}}{2\zeta_{\mathrm{j+1/2}}\Delta\lambda}, \tag{24b}$$

where

$$\bar{h}_{\mathrm{i+1/2,j}} = \frac{1}{2}\left(h_{\mathrm{i,j}} + h_{\mathrm{i+1,j}}\right), \qquad \bar{h}_{\mathrm{i,j+1/2}} = \frac{1}{2}\left(h_{\mathrm{i,j}} + h_{\mathrm{i,j+1}}\right), \tag{25}$$

and

$$\bar{T}_{\mathrm{i+1/2,j\pm1}} = \frac{1}{2}\left(T_{\mathrm{i,j\pm1}} + T_{\mathrm{i+1,j\pm1}}\right), \qquad \bar{T}_{\mathrm{i\pm1,j+1/2}} = \frac{1}{2}\left(T_{\mathrm{i\pm1,j}} + T_{\mathrm{i\pm1,j+1}}\right). \tag{26}$$

The coefficient $\zeta_{\mathrm{j+1/2}}$ in (24b) is given by $\zeta_{\mathrm{j+1/2}} = \sin\phi_{\mathrm{j+1/2}} \cos\phi_{\mathrm{j+1/2}}$. The zonal and meridional components of the saline contribution to the geostrophic velocity (14) are computed from similar equations.

The interior velocity at the base of the transition zone, (15), is computed from

$$w_{I,\mathrm{i,j}} = \frac{\bar{h}_{\mathrm{i+1/2,j}} u_{\mathrm{i+1/2,j}} - \bar{h}_{\mathrm{i\text{-}1/2,j}} u_{\mathrm{i\text{-}1/2,j}}}{r\cos\phi_{\mathrm{j}}\Delta\lambda} + \frac{\left(\bar{h}_{\mathrm{i,j+1/2}} v_c\right)_{\mathrm{i,j+1/2}} - \left(\bar{h}_{\mathrm{i,j\text{-}1/2}} v_c\right)_{\mathrm{i,j\text{-}1/2}}}{r\left(\sin\phi_{\mathrm{j+1/2}} - \sin\phi_{\mathrm{j\text{-}1/2}}\right)\Delta\phi}. \tag{27}$$

Finally, the open boundary condition (16) is discretized as

$$\frac{T^{n+1}_{\mathrm{i,j}} - T^{n}_{\mathrm{i,j}}}{\Delta t} = \frac{w_A}{h^n_{\mathrm{i,j}}}\left(T^n_{A,\mathrm{i,j}} - T^n_{\mathrm{i,j}}\right). \tag{28}$$

4.2.7 Solution for the Modern North Atlantic

In this section, we illustrate the ML temperature distribution and surface circulation in the modern North Atlantic that are simulated by the model and compare briefly the model solution with observational estimates. The ML temperature equation (7) is integrated to steady state using the numerical method described in the previous section and with values of $(T_A, T_I, S, h, \boldsymbol{\tau}_s)$ derived from modern climatologies (Appendix A). The initial conditions are provided by modern mean SSTs (*WOA*, 2013) averaged in model grid cells. The parameters of the ML model are listed in Table 1.

The simulated ML temperature distribution (Fig. 5) shows a modest adjustment compared to the initial conditions (Fig. 1), which reflects the fact that T_A is based on the modern SSTs (Appendix A) and the importance of surface flux in the ML heat balance (7). The importance of surface heat flux suggests that the open boundary condition (16) provides a reasonable approximation of the ML heat balance in the interior of the domain.

The simulated distribution of ML total velocity, $\bar{\mathbf{u}} = \bar{\mathbf{u}}_e + \bar{\mathbf{u}}_T + \bar{\mathbf{u}}_S$, shows a generally southeastward flow (Fig. 5a). This flow reveals the Ekman contribution to $\bar{\mathbf{u}}$ in our North Atlantic domain, where the zonal component of surface wind stress is predominantly eastward (*Risien and Chelton*, 2008). Temperature and salinity tend to offset their effects on horizontal density gradients and hence on the geostrophic contribution to $\bar{\mathbf{u}}$ (not shown). This result is consistent with observational studies showing that large-scale fronts in the North Atlantic are partially compensated, with waters tending to be warm and salty on one side of the fronts and cool and fresh on the other side (*Stommel*, 1993; *Chen*, 1995).

Observational estimates of North Atlantic surface circulation are derived from drifters which have drogues attached at depth (100 m or 15 m) to minimize the effects of the winds, whether direct or indirect through the Ekman currents (*Rossby*, 1996; *Fratantoni*, 2001)). In order to compare consistently these estimates with our model, we consider the simulated distribution of $\bar{\mathbf{u}}_T + \bar{\mathbf{u}}_S$, which is the geostrophic part of the total ML velocity (Fig. 5b). The simulated field of $\bar{\mathbf{u}}_T + \bar{\mathbf{u}}_S$ reveals a generally northeastward flow, which agrees qualitatively with the dritfer observations.

Notice that agreement is not found throughout the domain, however. In the region between 40°–50°W and 40°–50°N, the simulated velocity $\bar{\mathbf{u}}_T + \bar{\mathbf{u}}_S$ (Fig. 5b) does not reproduce the northward flow along the continental rise and the anticyclonic eddy (the 'Mann eddy'; *Mann*, 1967) southeast of the Grand Banks, as inferred from drifters (e.g., *Fratantoni*, 2001). In this region, the mean speed of surface current estimated from drifters (38 cm s^{-1}; *Fratantoni*, 2001) exceeds the simulated values of $|\bar{\mathbf{u}}_T + \bar{\mathbf{u}}_S|$ by one order of magnitude. Among the possible sources of disagreement are the model approximations and coarse horizontal resolution.

4.3 Sequential Methods

Sequential methods are coded in order to combine the sediment SST records (section 4.1) with the ocean ML model (section 4.2). The objective of this specific analysis is to produce an estimate of the time-dependent state of the surface North Atlantic over the past 14.5 kyrs which is consistent both observationally and dynamically. For conciseness, the problem of estimating past ocean states is referred to as the inverse problem.

4.3.1 State Vector

The elements of the state vector are the variables that define the state of the surface North Atlantic in terms of the model. They are the unknowns of the inverse problem, including the distributions of the ML temperature, the apparent atmospheric temperature, the interior temperature, the ML depth, and the Ekman and saline contributions to $\bar{\mathbf{u}}$. The thermal contribution to $\bar{\mathbf{u}}$ is not considered as a separate variable, since it can be determined diagnostically from the ML temperature field using (13).

The state vector ($\mathbf{x}$ below) is more specifically defined as follows. Let $\bar{u}_*$ and $\bar{v}_*$ be, respectively, the zonal and meridional component of the vector sum $\bar{\mathbf{u}}_e + \bar{\mathbf{u}}_S$. The apparent atmospheric temperature (T_A), the interior temperature (T_I), the ML depth (h), and the velocity components ($\bar{u}_*, \bar{v}_*$) are each a function of longitude (λ), latitude (ϕ), and time (t). The inclusion in the state vector of the gridded field of all these variables, however, would lead to a vector $\mathbf{x}$ with a dimension of $\mathrm{O}(10^3)$, which would make the application of sequential methods impractical given the computational and storage resources that are typically available.

In order to lower the dimension of $\mathbf{x}$, a 'state reduction' approach is adopted, whereby variables in $\mathbf{x}$ are approximated by analytic functions of spatial coordinates (e.g., *Gaspar and Wunsch*, 1989). The variables ($T_A, T_I, h, \bar{u}_*, \bar{v}_*$) are each represented as the sum of a

polynomial function and a residual term,

$$\begin{pmatrix} T_A \\ T_I \\ h \\ \bar{u}_* \\ \bar{v}_* \end{pmatrix} = \sum_{k=1}^{K} \begin{pmatrix} c_k^{(T_A)}(t) \\ c_k^{(T_I)}(t) \\ c_k^{(h)}(t) \\ c_k^{(\bar{u}_*)}(t) \\ c_k^{(\bar{v}_*)}(t) \end{pmatrix} \lambda_c^{a_k} \phi_c^{b_k} + \begin{pmatrix} \tilde{T_A} \\ \tilde{T_I} \\ \tilde{h} \\ \tilde{\bar{u}}_* \\ \tilde{\bar{v}}_* \end{pmatrix}. \tag{29}$$

Here $c_k^{(\cdot)}$ is a time-dependent coefficient, $\lambda_c = \lambda - \lambda_0$ and $\phi_c = \phi - \phi_0$, with $\lambda_0 = 29°\text{W}$ and $\phi_0 = 49°\text{N}$ being the central longitude and latitude of the domain, (a_k, b_k) are integral exponents, and $\tilde{(\cdot)}$ is a residual term that varies with (λ, ϕ). The coefficients $(c_k^{(T_A)}, c_k^{(T_I)}, c_k^{(h)}, c_k^{(\bar{u}_*)}, c_k^{(\bar{v}_*)})$ constitute the time-dependent part of the distributions of $(T_A, T_I, h, \bar{u}_*, \bar{v}_*)$. Their temporal evolution is described in probabilistic terms (random walk),

$$c_k^{(\cdot)}(t + \Delta t) = c_k^{(\cdot)}(t) + \eta_{c_k^{(\cdot)}}(t + \Delta t), \tag{30}$$

where $\eta_{c_k^{(\cdot)}}$ is a purely random process (noise) with zero mean and constant variance. The effect of this description is to impose some temporal covariance and non-stationarity on $(c_k^{(T_A)}, c_k^{(T_I)}, c_k^{(h)}, c_k^{(\bar{u}_*)}, c_k^{(\bar{v}_*)})$. The state vector is then defined as including the gridded field of ML temperature (including the T values at the boundaries) and the coefficients $c_k^{(\cdot)}$, $k = 1, 2, \cdots, K$,

$$\mathbf{x} = (T_{1,1}, \cdots, c_1^{(T_A)}, \cdots, c_1^{(T_I)}, \cdots, c_1^{(h)}, \cdots, c_1^{(\bar{u}_*)}, \cdots, c_1^{(\bar{v}_*)}, \cdots)', \tag{31}$$

where the time-dependency of the state elements is implicit and where the prime designates the vector transpose. The substitution in the state vector of the gridded fields of $(T_A, T_I, h, \bar{u}_*, \bar{v}_*)$ by their respective polynomial coefficients can reduce the dimension of the state vector very significantly, depending on K. For the results illustrated in this document, these fields are approximated with $K = 10$ terms (Table 2), which lowers the dimension of the state vector to 306 elements.

4.3.2 Observation and Dynamic Equations

The state vector $\mathbf{x}$ satisfies two equations, both of which are written below in discrete form, e.g., $\mathbf{x}(t)$ is written as $\mathbf{x}_i$, where i is a time index (equivalent to n in section 4.2.6).

The first equation is the observation equation,

$$\mathbf{z}_i = \mathbf{H}_i \mathbf{x}_i + \mathbf{v}_i, \tag{32}$$

where $\mathbf{z}_i$ is a vector of observations, $\mathbf{H}_i$ is a matrix that relates the state elements to the observations, and $\mathbf{v}_i$ is a vector of observational errors. In the present code, the observations are the sediment SST records (Fig. 2) and, for the modern time (0 yr BP), observational estimates of the elements of $\mathbf{x}$ derived from modern data. These estimates come from (i) the mean SSTs reported in (*WOA*, 2013) and (ii) the coefficients $(c_k^{(T_A)}, c_k^{(T_I)}, c_k^{(h)}, c_k^{(\bar{u}_*)}, c_k^{(\bar{v}_*)})$ estimated from modern observations (Appendix B).

The second equation satisfied by the state $\mathbf{x}$ is the dynamic equation,

$$\mathbf{x}_{i+1} = \mathbf{f}(\mathbf{x}_i) + \mathbf{w}_i, \tag{33}$$

where $\mathbf{f}$ is a vector of functions of $\mathbf{x}_i$ and $\mathbf{w}_i$ is another vector of errors. The functions in $\mathbf{f}$ are obtained from (i) the finite-difference approximations of the ML temperature equation at the interior points (19) and boundary points (28), and (ii) the probability model for the polynomial coefficients (30). Note that some of the finite-difference approximations in $\mathbf{f}$ contain products of state elements. As a result, some of the functions in $\mathbf{f}$ are nonlinear, and our inverse problem is a nonlinear (time-dependent) one.

4.3.3 Observation and Model Errors

Both the estimates of SST derived from the sediment records (section 4.1) and the ocean model considered for their interpretation (section 4.2) have sizeable uncertainties. Accordingly, neither the SST estimates nor the model equations should be imposed perfectly when analyzing the SST records. The following assumptions are made about the data errors, $\mathbf{v}_i$, and the model errors, $\mathbf{w}_i$. Both $\mathbf{v}_i$ and $\mathbf{w}_i$ are assumed to have zero mean and to show no temporal correlation. Moreover, they are taken to be mutually uncorrelated at any time. Collectively,

$$E[\mathbf{v}_i] = 0 \quad \text{and} \quad E[\mathbf{v}_i \mathbf{v}_j'] = \mathbf{R}_i \delta_{ij}, \tag{34a}$$

$$E[\mathbf{w}_i] = 0 \quad \text{and} \quad E[\mathbf{w}_i \mathbf{w}_j'] = \mathbf{Q}_i \delta_{ij}, \tag{34b}$$

$$E[\mathbf{v}_i \mathbf{w}_j'] = 0 \qquad \forall\ i, j, \tag{34c}$$

where $E[\cdot]$ is the mean (expected value) and δ_{ij} is the Kronecker delta, i.e., $\delta_{ij} = 1$ if $i = j$ and $\delta_{ij} = 0$ otherwise. The quantities $\mathbf{R}_i$ and $\mathbf{Q}_i$ are the covariance matrices for the observational errors and the model errors, respectively. These two matrices are described below.

The error covariance matrix $\mathbf{R}_i$ is constructed as follows. The diagonal elements of $\mathbf{R}_i$ are the error variances for the observations defined in $\mathbf{z}_i$, i.e., for the sediment SSTs and the modern observational estimates of the state elements. The error variances for the sediment SSTs are the square of the errors displayed in figure 2. The error variances for the modern SSTs are calculated by propagating the standard errors in the annual mean SSTs (*WOA*, 2013) contributing to the grid cell averages, assuming no error correlation. The error variances for the modern estimates of $(c_k^{(T_A)}, c_k^{(T_I)}, c_k^{(h)}, c_k^{(\bar{u}_*)}, c_k^{(\bar{v}_*)})$ are determined as described in appendix B. The off-diagonal elements of $\mathbf{R}_i$ are the error covariances for the observations in $\mathbf{z}_i$. They are set to zero, except for the modern estimates of $(c_k^{(T_A)}, c_k^{(T_I)}, c_k^{(h)}, c_k^{(\bar{u}_*)}, c_k^{(\bar{v}_*)})$ for which the error covariances are retained (Appendix B).

The error covariance matrix $\mathbf{Q}_i$ is established as follows. The diagonal elements of $\mathbf{Q}_i$ are the error variances for the equations defined in $\mathbf{f}(\mathbf{x}_i)$. They are assumed to be the same at every time, so that $\mathbf{Q}_i$ is time-invariant, i.e., $\mathbf{Q}_i = \mathbf{Q}$. The error variances for the discrete forms of the ML temperature equation at the interior points (19) and boundary points (28) are taken as proportional to the spatial average of annual mean SSTs in the model domain according to modern observations (*WOA*, 2013). This average is noted $\bar{T}_N$, where $i = N$ refers to the modern time (0 yr BP). Likewise, the variance of the noise in the probability model (30) is set proportional to the magnitude of $(c_k^{(T_A)}, c_k^{(T_I)}, c_k^{(h)}, c_k^{(\bar{u}_*)}, c_k^{(\bar{v}_*)})$ as estimated from modern observations. Thus,

$$\mathbf{Q} = \text{diag}\left(q^{(T)}, \cdots, q^{(T_A)}, \cdots, q^{(T_I)}, \cdots, q^{(h)}, \cdots, q^{(\bar{u}_*)}, \cdots, q^{(\bar{v}_*)}, \cdots\right), \tag{35}$$

where

$$\left(q^{(T)}, q^{(T_A)}, q^{(T_I)}, q^{(h)}, q^{(\bar{u}_*)}, q^{(\bar{v}_*)}\right) = \epsilon^2 \left(\bar{T}_N, \hat{c}_{k,N}^{(T_A)}, \hat{c}_{k,N}^{(T_I)}, \hat{c}_{k,N}^{(h)}, \hat{c}_{k,N}^{(\bar{u}_*)}, \hat{c}_{k,N}^{(\bar{v}_*)}\right)^2. \tag{36}$$

The factor ϵ is determined a posteriori, as described in section 4.4.1. The off-diagonal elements of $\mathbf{Q}_i$ are the error covariances for the equations in $\mathbf{f}(\mathbf{x}_i)$. They are set to zero,

i.e., the correlation between errors from different equations that may occur at a given time is neglected.

4.3.4 Kalman Filters

The conventional Kalman filter assumes that the equations in $\mathbf{f}$ and the observations in $\mathbf{z}$ are linear functions of the state elements in $\mathbf{x}$ (*Gelb et al.*, 1974; *Bryson and Ho*, 1975; *Anderson and Moore*, 1979). Consequently, it cannot be applied here given the nonlinearities in some of the equations. Different versions of the Kalman filter have been proposed in order to account for the presence of nonlinearities in the system dynamics and (or) in the observations (for a short review see *Wunsch* (2006)). Two of these versions are implemented in the code: the Extended Kalman Filter (EKF) and the Linearized Kalman Filter (LKF). Both versions rely on the linearization of the equations in $\mathbf{f}$, but around a different state. In the EKF, the equations in $\mathbf{f}(\mathbf{x}_i)$ are linearized about the most recent state estimate at time i. In the LKF, they are linearized about a reference state, which in the present code is a constant state constrained from modern observations.

The following notation is introduced before describing the EKF and LKF. The Kalman filter estimate of the state at time i is denoted as $\hat{\mathbf{x}}_i(+)$, where the plus sign indicates that the estimate considers the data prior to and at time i. This notation is used to contrast $\hat{\mathbf{x}}_i(+)$ from $\hat{\mathbf{x}}_i(-)$, which is the estimate at time i that only considers the data prior to this time. The error covariance matrix, or uncertainty, of $\hat{\mathbf{x}}_i(\pm)$ is noted $\mathbf{P}_i(\pm) = E[\hat{\mathbf{x}}_i(\pm) - \mathbf{x}_i)(\hat{\mathbf{x}}_i(\pm) - \mathbf{x}_i)']$, where $\mathbf{x}_i$ is the true state at time i.

For the present application of the code, the initial state estimate at 14,500 yr BP, $\hat{\mathbf{x}}_0(+)$, and its uncertainty, $\mathbf{P}_0(+) = E[(\hat{\mathbf{x}}_0(+) - \mathbf{x}_0)(\hat{\mathbf{x}}_0(+) - \mathbf{x}_0)']$, are determined as follows. Consider first $\hat{\mathbf{x}}_0(+)$. The initial SST field is obtained by averaging in model grid cells the modern annual mean SSTs which are available at $1^\circ \times 1^\circ$ horizontal resolution in *WOA* (2013). The initial coefficients $(c_k^{(T_A)}, c_k^{(T_I)}, c_k^{(h)}, c_k^{(\bar{u}_*)}, c_k^{(\bar{v}_*)})$ are determined from modern observations as described in appendix B. Consider then $\mathbf{P}_0(+)$. The error variances for the initial SSTs are set equal to the spatial variance of the annual mean SSTs in the domain

which are used for the initial SST field. The error covariances in the initial SST field are taken as zero. The error (co)variances for the initial coefficients ($c_k^{(T_A)}, c_k^{(T_I)}, c_k^{(h)}, c_k^{(\bar{u}_*)}, c_k^{(\bar{v}_*)}$) are derived from the errors in modern observations (Appendix B).

Extended Kalman Filter In the EKF, the equations in $\mathbf{f}[\mathbf{x}_i]$ are linearized about the more recent estimate of the state, $\hat{\mathbf{x}}_i(+)$, in the calculation of state error propagation,

$$\mathbf{f}[\mathbf{x}_i] = \mathbf{f}[\hat{\mathbf{x}}_i(+)] + \frac{\partial \mathbf{f}}{\partial \mathbf{x}}|_{\hat{\mathbf{x}}_i(+)} \left(\mathbf{x}_i - \hat{\mathbf{x}}_i(+)\right), \tag{37}$$

where $(\partial \mathbf{f}/\partial \mathbf{x})|_{\hat{\mathbf{x}}_\mathbf{i}(+)}$ is a matrix of partial derivatives evaluated at $\mathbf{x}_i = \hat{\mathbf{x}}_i(+)$ (Appendix C). Like other versions of the Kalman filter, the EKF consists of two sets of equations. In the first set (the time-update equations), the model is used to extrapolate the state and its uncertainty from time $i-1$ to time i:

$$\hat{\mathbf{x}}_i(-) = \mathbf{f}\left[\hat{\mathbf{x}}_{i-1}(+)\right], \tag{38a}$$

$$\mathbf{P}_i(-) = \frac{\partial \mathbf{f}}{\partial \mathbf{x}}|_{\hat{\mathbf{x}}_{i-1}(+)} \mathbf{P}_{i-1}(+) \left[\frac{\partial \mathbf{f}}{\partial \mathbf{x}}|_{\hat{\mathbf{x}}_{i-1}(+)}\right]' + \mathbf{Q}. \tag{38b}$$

The state error evolution (38b) is governed by two terms. The first term on the right-hand side represents the effect of dynamic system stability. Broadly, a very stable system will tend to cause this term to be smaller than $\mathbf{P}_{i-1}(+)$, whereas an unstable system will experience unbounded error growth in the absence of observations (*Gelb et al.*, 1974). The second term on the right of (38b) represents the effect of model errors. For example, for $\epsilon = 10^{-3}$ in (36), the error in ML temperature would tend to increase by an amount equal to $10^{-3}\sqrt{q^{(T)}} = 10^{-3}\bar{T}_N$ in one time step in the absence of observations. With a time step of 0.05 yr^{-1} (0.1 yr^{-1}), which are the values used for the model integrations, the ML temperature errors tend to grow by an amount equal to $\bar{T}_N$ in 50 yr (100 yr), should no observations be available over this interval.

In the second set of equations (the data-update equations), the extrapolated state and its uncertainty are modified in order to account for the presence of observations (if no observation is available, then the state and its uncertainty keep evolving according to (38a–38b)). A state estimate is sought which minimizes the objective function

$$J = \left(\hat{\mathbf{x}}_i(-) - \mathbf{x}_i\right)' \mathbf{P}_i(-)^{-1} \left(\hat{\mathbf{x}}_i(-) - \mathbf{x}_i\right) + \left(\mathbf{z}_i - \mathbf{H}_i\mathbf{x}_i\right)' \mathbf{R}_i^{-1} \left(\mathbf{z}_i - \mathbf{H}_i\mathbf{x}_i\right). \tag{39}$$

The first term on the right represents the deviation from the extrapolated state, $\hat{\mathbf{x}}_i(-)$, and the second represents the deviation from the observations, $\mathbf{z}_i$, weighted by the error covariances $\mathbf{P}_i(-)$ and $\mathbf{R}_i$, respectively. The resulting state estimate and its uncertainty are given by the data-update equations:

$$\hat{\mathbf{x}}_i(+) = \hat{\mathbf{x}}_i(-) + \mathbf{K}_i \left[\mathbf{z}_i - \mathbf{H}_i \hat{\mathbf{x}}_i(-)\right], \tag{40a}$$

$$\mathbf{P}_i(+) = \left[\mathbf{I} - \mathbf{K}_i \mathbf{H}_i\right] \mathbf{P}_i(-) \left[\mathbf{I} - \mathbf{K}_i \mathbf{H}_i\right]' + \mathbf{K}_i \mathbf{R}_i \mathbf{K}_i', \tag{40b}$$

where

$$\mathbf{K}_i = \mathbf{P}_i(-)\mathbf{H}_i' \left[\mathbf{H}_i \mathbf{P}_i(-) \mathbf{H}_i' + \mathbf{R}_i\right]^{-1}, \tag{41}$$

is the Kalman gain. Thus, the Kalman filter estimate (40a) is a weighted least-squares estimate, where the weighting is provided by $\mathbf{P}_i(-)$ and $\mathbf{R}_i$ (e.g., *Bryson and Ho*, 1975; *Stengel*, 1986; *Brogan*, 1991; *Wunsch*, 2006). Notice that (40b) is used here rather than the simpler and mathematically equivalent form $\mathbf{P}_i(+) = [\mathbf{I} - \mathbf{K}_i \mathbf{H}_i]\mathbf{P}_i(-)$, as it tends to promote nonnegativity of $\mathbf{P}_i(+)$ (e.g., *Anderson and Moore*, 1979).

The EKF has been found to yield accurate estimates in number of applications and reduces to the conventional Kalman filter when the system dynamics and the observations are linear. For these reasons, the EKF is usually one of the first methods to be tried for any nonlinear filtering problem (e.g., *Gelb et al.*, 1974). On the other hand, the EKF may be prone to instabilities (e.g., *Wunsch*, 2006) and indeed failed to produce consistently stable results for the present problem (not shown). Another version of the Kalman filter that can deal with nonlinearities, the LKF, is considered as an alternative method to combine the SST records with the ocean model.

Linearized Kalman Filter In the LKF, the state vector is represented as the sum of a nominal or reference state, $\mathbf{x}_i^0$, and a perturbation, $\delta \mathbf{x}_i$,

$$\mathbf{x}_i = \mathbf{x}_i^0 + \delta \mathbf{x}_i, \tag{42}$$

and the model equations are linearized about the reference state,

$$\mathbf{f}(\mathbf{x}_i) = \mathbf{f}(\mathbf{x}_i^0) + \frac{\partial \mathbf{f}}{\partial \mathbf{x}}|_{\mathbf{x}_i^0} \, \delta \mathbf{x}_i. \tag{43}$$

The time-update equations of the LKF are

$$\delta\hat{\mathbf{x}}_i(-) = \frac{\partial \mathbf{f}}{\partial \mathbf{x}}|_{\mathbf{x}_i^0}\, \delta\hat{\mathbf{x}}_{i-1}(+), \tag{44a}$$

$$\mathbf{P}_i(-) = \frac{\partial \mathbf{f}}{\partial \mathbf{x}}|_{\mathbf{x}_i^0}\, \mathbf{P}_{i-1}(+) \left[\frac{\partial \mathbf{f}}{\partial \mathbf{x}}|_{\mathbf{x}_i^0}\right]' + \mathbf{Q}, \tag{44b}$$

whereas the data-update equations of the filter are

$$\delta\hat{\mathbf{x}}_i(+) = \delta\hat{\mathbf{x}}_i(-) + \mathbf{K}_i\left[\delta\mathbf{z}_i - \mathbf{H}_i\delta\hat{\mathbf{x}}_i(-)\right] \tag{45}$$

and the equation for $\mathbf{P}_i(+)$, which has the same form as (40b). In (45), the gain $\mathbf{K}_i$ is computed from (41) and $\delta\mathbf{z}_i$ is the vector difference $\mathbf{z}_i - \mathbf{H}_i\mathbf{x}_i^0$.

For the present problem, the reference state, $\mathbf{x}_i^0$, is taken as time-independent and is obtained from modern observations. Thus, $\mathbf{x}_i^0 = \hat{\mathbf{x}}_0(+)$, so that $\delta\hat{\mathbf{x}}_0(+) = \mathbf{0}$. A more plausible reference state would require prior knowledge about the past evolution of the distributions of SST, ML depth, surface wind stress, etc., which is not available. In general, the LKF is not expected to yield accurate state estimates if the state drifts very far from the reference state. In such a situation, the EKF, which uses model equations linearized about the most recent state estimate, can be more accurate.

4.3.5 Linearized Smoother

A Kalman filter constitutes an incomplete analysis, in the sense that the filter estimates are based solely on past and present observations: the filter estimate $\hat{\mathbf{x}}_i(+)$ is determined from data prior to and at time i but is not constrained by observations posterior to time i. In order to account for posterior observations (if any), a smoother should be used (*Gelb et al.*, 1974; *Bryson and Ho*, 1975; *Anderson and Moore*, 1979).

A Linearized Smoother (LS) is implemented in the code. Application of the LS to our problem allowed us to estimate states of the surface North Atlantic over the past 14.5 kyrs that are consistent with the entire SST records and the modern observations, as well as with the model physics. Since past ocean states are generally to be estimated at times within a fixed interval, a so-called fixed-interval smoother is applied (*Gelb et al.*, 1974; *Anderson and Moore*, 1979).

The smoother equations used in this study are based on an algorithm originally developed for linear systems and reported in *Bryson and Ho* (1975) (p. 392) (see also *Fraser*, 1967). An estimate of the state perturbation, $\delta\mathbf{x}_i$, is sought which minimizes

$$\begin{aligned} J &= (\delta\hat{\mathbf{x}}_0(+) - \delta\mathbf{x}_0)' \mathbf{P}_0(+)^{-1} (\delta\hat{\mathbf{x}}_0(+) - \delta\mathbf{x}_0) \\ &+ \sum_{i=1}^{N} (\delta\mathbf{z}_i - \mathbf{H}_i\delta\mathbf{x}_i)' \mathbf{R}_i^{-1} (\delta\mathbf{z}_i - \mathbf{H}_i\delta\mathbf{x}_i) \\ &+ \sum_{i=0}^{N-1} \mathbf{w}_i'\mathbf{Q}^{-1}\mathbf{w}_i, \end{aligned} \tag{46}$$

subject to the constraint $\delta\mathbf{x}_{i+1} = [\partial\mathbf{f}/\partial\mathbf{x}|_{\hat{\mathbf{x}}_0(+)}]\delta\mathbf{x}_i + \mathbf{w}_i$. The resulting, smoothed estimate is given by

$$\delta\hat{\mathbf{x}}_i = \delta\hat{\mathbf{x}}_i(+) - \mathbf{P}_i(+) \left[\frac{\partial\mathbf{f}}{\partial\mathbf{x}}|_{\hat{\mathbf{x}}_0(+)}\right]' \mathbf{l}_i, \tag{47}$$

where

$$\mathbf{l}_{i-1} = (\mathbf{I} - \mathbf{P}_i(+)\mathbf{S}_i)' \left(\left[\frac{\partial\mathbf{f}}{\partial\mathbf{x}}|_{\hat{\mathbf{x}}_0(+)}\right]' \mathbf{l}_i - \mathbf{H}_i'\mathbf{R}_i^{-1} [\delta\mathbf{z}_i - \mathbf{H}_i\delta\hat{\mathbf{x}}_i(-)] \right), \tag{48}$$

with the terminal condition $\mathbf{l}_N = \mathbf{0}$ and with $\mathbf{S}_i = \mathbf{H}_i'\mathbf{R}_i^{-1}\mathbf{H}_i$. The first term on the right-hand side of (47) is the state perturbation estimated by the LKF. The second is a correction which is proportional to a vector, $\mathbf{l}_i$, driven by posterior data according to the recursion formula (48). The state estimate (47) is thus constrained by the entire set of observations, from the initial time ($i = 0$) to the terminal time ($i = N$). As for the Kalman filter estimates, the smoother estimates can be regarded as weighted least-squares estimates, but with the weighting now provided by $\mathbf{P}_0(+)$, $\mathbf{R}_i$, and $\mathbf{Q}$ over the entire interval (*Bryson and Ho*, 1975).

The uncertainty in the smoothed estimate (47) is given by

$$\mathbf{P}_i = \mathbf{P}_i(+) - \mathbf{P}_i(+) \left[\frac{\partial\mathbf{f}}{\partial\mathbf{x}}|_{\hat{\mathbf{x}}_0(+)}\right]' \mathbf{L}_i \frac{\partial\mathbf{f}}{\partial\mathbf{x}}|_{\hat{\mathbf{x}}_0(+)} \mathbf{P}_i(+), \tag{49}$$

where

$$\mathbf{L}_{i-1} = (\mathbf{I} - \mathbf{P}_i(+)\mathbf{S}_i)' \left[\frac{\partial\mathbf{f}}{\partial\mathbf{x}}|_{\hat{\mathbf{x}}_0(+)}\right]' \mathbf{L}_i \frac{\partial\mathbf{f}}{\partial\mathbf{x}}|_{\hat{\mathbf{x}}_0(+)} (\mathbf{I} - \mathbf{P}_i(+)\mathbf{S}_i) + \mathbf{S}_i (\mathbf{I} - \mathbf{P}_i(+)\mathbf{S}_i), \tag{50}$$

with the terminal condition $\mathbf{L}_N = \mathbf{0}$. The first term on the right-hand side of (49) is the state uncertainty obtained from the LKF. The second term is always positive-definite, indicating that the errors in the state estimates generally decrease as posterior data are

considered in the analysis (more precisely, these errors never increase). This term depends on the matrix $\mathbf{L}_i$, which accounts for the errors in the posterior data represented in $\mathbf{S}_i$ and which is calculated by recursion (50).

The algorithm (47–50) is mathematically equivalent to the Rauch-Tung-Striebel (RTS) algorithm (*Rauch et al.*, 1965), a conventional method for fixed-interval smoothing (*Gelb et al.*, 1974; *Bryson and Ho*, 1975; *Anderson and Moore*, 1979). The two algorithms differ in the matrix inversions: whereas the RTS requires the calculation of $\mathbf{P}_i(-)^{-1}$, equations (47–50) rely on $\mathbf{R}_i^{-1}$. Since for the present problem $\mathbf{R}_i$ is generally of much smaller order than $\mathbf{P}_i(-)$, equations (47–50) offer a clear numerical advantage.

4.4 Examples of Filtered and Smoothed Solutions

4.4.1 LKF Solution

In this section, the LKF is applied to estimate the time-dependent state of the surface North Atlantic over the entire time interval from 14,500 yr BP ($i = 0$) to 0 yr BP ($i = N$). We illustrate the effect of model errors on the state estimates and present a solution that will constitute the first part of the smoothing solution to be discussed in section 4.4.3.

The application of a Kalman filter such as LKF requires knowledge of the covariance matrices for the data and model errors. In general, whereas data errors are relatively well-constrained, model errors are more poorly understood. However, the sequence $\delta\mathbf{z}_i - \mathbf{H}_i\delta\hat{\mathbf{x}}_i(-) = \mathbf{z}_i - \mathbf{H}_i\hat{\mathbf{x}}_i(-)$ contains information about the ability of the model to replicate observations and hence about model errors. Consider a linear and time-invariant system, i.e., a system with $\mathbf{z}_i = \mathbf{H}\mathbf{x}_i + \mathbf{v}_i$ and $\mathbf{f}(\mathbf{x}_i) = \mathbf{A}\mathbf{x}_i + \mathbf{b}_i$, where $(\mathbf{A}, \mathbf{H}, \mathbf{R}, \mathbf{Q})$ are constant matrices and $\mathbf{b}_i$ is a deterministic forcing. A filter of such a system is optimal provided that $\mathbf{z}_i - \mathbf{H}\hat{\mathbf{x}}_i(-)$ is a normal white noise sequence with variance $\mathbf{H}'\mathbf{P}_i(-)\mathbf{H} + \mathbf{R}$ (*Mehra*, 1970). The properties of $\mathbf{z}_i - \mathbf{H}\hat{\mathbf{x}}_i(-)$, known as the innovation sequence, can therefore be consulted in order to assess the optimality of the filtering solution. Although the system (32–33) is not linear and not time-invariant (e.g., $\mathbf{H} = \mathbf{H}_i$ is variable), the innovation properties are nonetheless useful for evaluating the ability of the model to explain the observations and for constraining a plausible choice of model errors in $\mathbf{Q}$, as shown below.

We consider three solutions of the LKF obtained from different assumptions about the model errors in $\mathbf{Q}$: $\epsilon = 10^{-4}$, $\epsilon = 10^{-3}$, and $\epsilon = 10^{-2}$. For each solution, we illustrate both the elements of $\mathbf{z}_i - \mathbf{H}_i\hat{\mathbf{x}}_i(-)$ (Fig. 6) and the distribution function of these elements normalized to their standard deviations (Fig. 7). Note that the elements of $\mathbf{z}_N - \mathbf{H}_N\hat{\mathbf{x}}_N(-)$, which includes modern observations, are removed from both figures in order to isolate the ability of the model to replicate the sediment SST records.

For the solution with $\epsilon = 10^{-4}$ (relatively small model errors), the elements of $\mathbf{z}_i - \mathbf{H}_i\hat{\mathbf{x}}_i(-)$ average –0.8°C with a standard error of 0.1°C (Fig. 6a), suggesting a negative bias: the

SST records are poorly replicated, indicating that the model errors are assumed to be too small in this case (Fig. 7a). In contrast, for the solution with $\epsilon = 10^{-2}$ (higher model errors), the innovation elements average 0.1°C with a standard error of 0.1°C (Fig. 6c), revealing no apparent bias. However, the close fit of the filtered ML temperatures to the sediment SSTs that is obtained in this case does not seem to be warranted given the errors in the sediment SSTs (Fig. 7c), suggesting that the choice $\epsilon = 10^{-2}$ is giving too much confidence in the data. The intermediate choice $\epsilon = 10^{-3}$ leads to a solution that shows both no clear bias (Fig. 6b) and no clear sign of under- or over-fit to the SST records (Fig. 7b).

The time series of ML temperature near the sediment core locations as estimated by the LKF for $\epsilon = 10^{-3}$ are shown in Figure 8. As expected, the temperatures estimated from filtering are generally consistent with those reconstructed from the faunal counts for each core: the differences between the filtered and reconstructed temperatures are generally less than one standard deviation in the filtered estimates.

Notice the discontinuities in the time series of the filtered temperatures and of their errors, which occur when SST observations are available (Fig. 8). When observations are available, the filter combines the model forecast, $\delta\hat{\mathbf{x}}_i(-)$, with the observations, $\delta\mathbf{z}_i$, to produce the filter estimate, $\delta\hat{\mathbf{x}}_i(+)$, according to (45). The state then deviates from its evolution driven by the model to a degree that depends on the Kalman gain, i.e., on the relative 'magnitude' of $\mathbf{P}_i(-)$ and $\mathbf{R}_i$. The error in the filter temperature estimate is reduced when observations are available (Fig. 8). This behaviour can be understood from the following equation,

$$\mathbf{P}_i(+)^{-1} = \mathbf{P}_i(-)^{-1} + \mathbf{H}_i'\mathbf{R}_i\mathbf{H}_i, \tag{51}$$

which can be derived from $\mathbf{P}_i(+) = [\mathbf{I} - \mathbf{K}_i\mathbf{H}_i]\mathbf{P}_i(-)$ using the matrix inversion lemma (*Liebelt*, 1967). As shown by (51), the uncertainty of the state after measurement, $\mathbf{P}_i(+)$, is never larger than $\mathbf{P}_i(-)$ since $\mathbf{H}_i'\mathbf{R}_i\mathbf{H}_i$ is at least positive-definite (*Bryson and Ho*, 1975). In contrast, when observations are not available, the evolution of the state is entirely governed by the model (44a) and the state uncertainty evolves according to the error propagation equation (44b).

4.4.2 Comparing EKF and LKF Solutions

We compare the ML temperature estimates obtained from the EKF and LKF near the sediment core locations for the time interval between 10–14.5 kyr BP. This interval is characterized by the largest temperature changes over the past 14.5 kyr BP in the sediment records (Fig. 2). It is therefore the interval when the largest differences between the results from both filters can reasonably be expected, given the varying assumptions in both methods. To ensure comparability of the results, the equations of the EKF and LKF are solved with the same assumptions about $\mathbf{R}_i$ and $\mathbf{Q}$ ($\epsilon = 10^{-3}$). On the other hand, a time step of $\Delta t = 0.05$ yr is used for the EKF, compared to $\Delta t = 0.1$ yr for the LKF. Indeed, EKF experiments with time steps $\Delta t > 0.05$ yr led to unstable solutions (not shown).

It is seen that the ML temperature estimates derived from the EKF and LKF show small differences: the estimates derived from the extended filter differ from those derived from the linearized filter by less than one standard deviation of either the EKF or LKF estimates (Figs. 9–10). Likewise, the standard deviations in the ML temperature estimates obtained from both methods are generally comparable (Fig. 10). Thus, at least for the present problem and with the present assumptions about the error covariances, the EKF and LKF seem to lead to similar estimates of time-dependent states.

4.4.3 Smoothed Solution

In this section, the Linearized Smoother is applied to estimate the time-dependent state of the surface North Atlantic over the past 14,500 yrs. The time series of ML temperature near the sediment core locations as estimated by the smoother are shown in figure 11. In contrast to the filtered estimates (Fig. 8), each smoothed estimate of temperature is constrained by the entire data set, including by the data posterior to the time of the estimate. The consideration of posterior data has two noticeable consequences. First, compared to the filtered estimates, the smoothed estimates of temperature present reduced discontinuities at times of data uptake, hence the name ‘smoother’. Second, the errors in

the smoothed estimates are lower than the errors in the filtered estimates, as anticipated from (49) (compare Fig. 11 with Fig. 8).

In order to illustrate the potential of sequential methods for paleoceanographic reconstructions, we illustrate the position of the 10°C ML isotherm in the North Atlantic domain during the Younger Dryas which is estimated in the smoothing solution (Fig. 12). As shown in this figure, the isotherm has a more zonal orientation and southerly position at 12,000 yr BP compared to today. Surface waters warmer than 10°C would have been confined to south of 48°N throughout the basin in the annual mean sense. The errors in the smoothed estimates of ML temperature at 12,000 yr BP vary from 0.54°C to 0.93°C, with minima in the latitude band between the sediment core locations and maxima outside the band (dashed lines in Fig. 12). This pattern results from a combination of model dynamics ($\mathbf{f}$), model errors ($\mathbf{Q}$), data distribution ($\mathbf{H}_i$), and data errors ($\mathbf{R}_i$), as shown by the error covariance equations of the filter (44b) and the smoother (49).

5 Computer Code

In this section, we present the computer code. The code includes a main program (*main.f*), a set of 27 routines, a file of shared variables (*commonvar.f*), and a file for the code compilation (*makefile*). Each of these entities are described in turn below.

5.1 Main Program

The main program of the code is called *main.f*. This program serves as a supervisor and coordinator of the tasks that are completed in the routines. The main program executes the following major operations. First, it reads information from a start file called *start.*[tag]. The extension [tag] is a user-defined character string (≤ 50 characters) that is employed to label many of the output files of the code. The main program then calls a set of routines in the following order:

opening.f This routine opens a number of output files.

setting.f This routines establishes the model grid, defines various indices for model grid points, and calculates parameters used for the evaluation of the partial derivatives in the matrix $\partial\mathbf{f}/\partial\mathbf{x}$.

iaxxxxx.f This routine assigns a character string to each variable of the state vector $\mathbf{x}$ and assigns 'binary coefficients' for a more efficient evaluation of the partial derivatives in $\partial\mathbf{f}/\partial\mathbf{x}$.

reading.f The main program calls this routine with 'reco' as an argument in order to read the sediment SST records.

selxxxx.f This routine selects the SST records and defines related quantities which are used in the code. It has been written to handle situations where only a subset of the records that are read in *reading.f* should be considered in the inversion.

mod-sta.f This routine returns an estimate of the modern state of the surface North Atlantic domain. This modern state is based either (i) entirely on observational estimates that are read from multiple calls to *reading.f* or (ii) on the numerical solution of the mixed-layer model obtained with modern values of apparent atmospheric temperature, interior temperature, mixed-layer depth, and zonal and meridional wind stresses.

fil-lkf.f This routine applies a Linearized Kalman Filter to combine the SST records with the advective mixed-layer model. It calls itself a large number of routines that are detailed later in this document.

fil-ekf.f This routine applies an Extended Kalman Filter to combine the SST records with the advective mixed-layer model. As for *fil-lkf.f*, it calls a large number of routines that are described later.

smoothe.f This routine applies a Linearized Smoother to combine the state estimates obtained from the Linearized Kalman Filter with posterior observations.

5.2 Routines

In this section, each routine of the code is described. A routine can be either a subroutine or a function. The code includes a total of 27 routines. Each routine starts with a set of comments that specifies (1) the job done by the routine, (2) the entity (main program or other routine) that calls the routine, and (3) the other routines that are called by the routine (secondary calls, if any). The number of secondary calls has been minimized in an effort to increase code legibility. An effort has also been made to force the user to define all variables used in the code by adding the statement **implicit none** at the beginning of the main program and of each routine. It is the author's experience that this statement is a very helpful device for finding coding errors. Following the statement **implicit none** is the statement **include 'commonvar.f'**. This second statement allows the variables declared in the file *commonvar.f* to be shared among the main program and all the routines that incorporate this statement. Each routine is briefly described below (in alphabetical order).

5.2.1 *coepoly.f*

This subroutine returns weighted least-squares estimates of the polynomial coefficients which appear in the representation (29),

$$\begin{pmatrix} T_A \\ T_I \\ h \\ \bar{u}_* \\ \bar{v}_* \end{pmatrix} = \sum_{k=1}^{K} \begin{pmatrix} c_k^{(T_A)}(t) \\ c_k^{(T_I)}(t) \\ c_k^{(h)}(t) \\ c_k^{(\bar{u}_*)}(t) \\ c_k^{(\bar{v}_*)}(t) \end{pmatrix} \lambda_c^{a_k} \phi_c^{b_k} + \begin{pmatrix} \tilde{T}_A \\ \tilde{T}_I \\ \tilde{h} \\ \tilde{\bar{u}}_* \\ \tilde{\bar{v}}_* \end{pmatrix}. \tag{52}$$

It must be called with one argument, [c6]. This 6-character string will select the physical variable for which these coefficients are to be estimated: the apparent temperature (T_A), the interior temperature (T_I), the ML depth (h), the ML zonal velocity $\bar{u}_*$, or the ML meridional ML velocity $\bar{v}_*$. The routine completes two main tasks. First, it casts the least-squares estimation problem in the canonical form

$$\mathbf{Ex} + \mathbf{n} = \mathbf{y},$$

where $\mathbf{E}$ is a coefficient matrix, $\mathbf{x}$ is a vector of unknowns (in our case, the polynomial coefficients), $\mathbf{y}$ is a vector of observations, and $\mathbf{n}$ is the vector of errors in these observations. In this first task, the routine fills in this matrix and these vectors. In the second task, it calculates the weighted-least squares estimates of $\mathbf{x}$ as well as the error covariances (Appendix B).

5.2.2 *df-dxxx.f*

This subroutine evaluates the partial derivatives of the model equations (their finite-difference forms) with respect to the state variables. These derivatives are the elements of the matrix $\partial\mathbf{f}/\partial\mathbf{x}$. The subroutine must be called with an argument, [nN], set equal to the order of this matrix. The derivatives of the ML temperature equations are evaluated first, followed by those of the polynomial coefficients for the apparent temperature, the interior temperature, the ML depth, the ML zonal velocity $\bar{u}_*$, and the ML meridional velocity $\bar{v}_*$:

> For the ML temperature equations at the interior points, the derivatives with respect to the ML temperatures and to the polynomial coefficients for T_A, T_I, h, $\bar{u}_*$, and $\bar{v}_*$ must be calculated. To avoid multiple testing and hence reduce computational time, the derivatives of the ML temperature equation at point (i, j) with respect to the ML temperatures at the point (i, j) and at the eight neighboring points are calculated using the binary coefficients that are previously assigned in the routine *iaxxxxx.f*.
>
> For the ML temperature equations at the boundary points, the derivatives with respect to the local ML temperature and to the polynomial coefficients for apparent temperature and ML depth must only be calculated.
>
> Finally, the derivative of the equation for a given polynomial coefficient (say, the first polynomial coefficient for apparent temperature) with respect to the same polynomial coefficient is assigned a value of one, consistent with the probability model (30). All the other derivatives of this equation are set to zero.

5.2.3 *EExxxxx.f*

This function returns an element of the coefficient matrix **E** of the set of linear algebraic equations

$$\mathbf{E}\mathbf{x} + \mathbf{n} = \mathbf{y}, \tag{53}$$

which derives from (29). Here **E** is a coefficient matrix, **x** is a vector of unknowns (the polynomial coefficients $c_k^{(\cdot)}$), **y** is a vector of observations, and **n** is the vector of errors in these observations. The routine *EExxxxx.f* is called with 4 arguments: [ni] is the coefficient number k of $c_k^{(\cdot)}$, [i] is the longitude index of the grid point, [j] is the latitude index of the grid point, and [c2] is the variable. For example, if *EExxxxx.f* is called with [ni=1] when the exponents a_1 and b_1 are both set equal to zero (Table 2), then *EExxxxx.f* returns the value $\lambda_c^0 \phi_c^0 = 1$. If *EExxxxx.f* is called with [ni=2] when a_2 is set to zero and b_2 is set to 1 (Table 2), then it returns the value $\lambda_c^0 \phi_c^1 = \phi_c$.

5.2.4 *fil-ekf.f*

This subroutine applies the Extended Kalman Filter to combine the observations and the model. It carries out the following main tasks. First, it initializes the filter by assigning values to different quantities, such as the initial state estimate, $\hat{\mathbf{x}}_0(+)$, its error covariance, $\mathbf{P}_0(+)$, and the error covariance for the model errors, **Q**. Second, it applies the EKF from an initial time to a final time defined by the integer [itot-fs] (time loop). The value of [itot-fs] must be set in the main program, *main.f*. Finally, the routine *fil-ekf.f* periodically writes out different results from multiple calls to *writing.f*.

5.2.5 *fil-lkf.f*

This subroutine applies the Linearized Kalman Filter to combine the observations and the model. It carries out a number of tasks. First, it initializes the filter by assigning values to different quantities, such as the initial state estimate ($\delta\hat{\mathbf{x}}_0(+)$), its error covariance, $\mathbf{P}_0(+)$, the error covariance matrix for the model errors, **Q**, and the matrix of partial

derivatives $\partial \mathbf{f}/\partial \mathbf{x}|_{\mathbf{x}=\hat{\mathbf{x}}_0(+)}$. Second, it writes out the prior ($\hat{\mathbf{x}}_0(-)$) and posterior ($\hat{\mathbf{x}}_0(+)$) estimates of the initial state, as well as the uncertainty in the posterior estimate of the initial state ($\mathbf{P}_0(+)$), which are later used by the Linearized Smoother. Third, it applies the LKF from an initial time to a final time defined by the integer [itot-fs] (time loop). The value of [itot-fs] must be set in the main program, *main.f*. Fourth, it writes out, at each time of the loop, the prior and posterior estimates of the state, respectively, $\hat{\mathbf{x}}_i(-)$ and $\hat{\mathbf{x}}_i(+)$, as well as the uncertainty in the posterior estimate of the state, $\mathbf{P}_i(+)$. These three quantities will also be used by the Linearized Smoother. Finally, the routine *fil-lkf.f* periodically writes out other results through multiple calls to *writing.f*.

5.2.6 *freezin.f*

This subroutines tests that the ML temperature, T, and the interior temperature, T_I, at boundary and interior grid points are not below the freezing point of seawater (–1.9°C).

5.2.7 *iaxxxxx.f*

This subroutine performs two tasks. First, it returns a 8-character string for each state variables in $\mathbf{x}$. These variables are (i) the ML temperature at all model grid points (T) and (ii) the polynomial coefficients for the apparent atmospheric temperature ($c_k^{(T_A)}$), the interior temperature ($c_k^{(T_I)}$), the ML depth ($c_k^{(h)}$), the ML zonal velocity $\bar{u}_*$ ($c_k^{(\bar{u}_*)}$), and the ML meridional velocity $\bar{v}_*$ ($c_k^{(\bar{v}_*)}$). Second, it assigns a value of 0 or 1 to each element of the three-dimensional integer array [ia(,,)]. This array is used to avoid the need for repeated testing in routine *df-dxxx.f*, where the partial derivatives in $\partial \mathbf{f}/\partial \mathbf{x}$ are evaluated.

5.2.8 *mod-int.f*

This subroutine solves the ML temperature equation using the numerical method described in section 4.2.6. It completes the following main tasks. First, it calculates the vertical interior velocities from a call to the routine *w-ixxxx.f*. Second, it computes the

temperature changes in one time step at interior and then boundary points. Finally, it adds the temperature changes to the previous ML temperature field.

5.2.9 *mod-sta.f*

This subroutine returns an estimate of the modern state of the surface North Atlantic. It carries out the following main tasks. First, it reads modern observations of ML temperature, ML salinity, apparent atmospheric temperature, interior temperature, ML depth, and zonal wind and meridional wind stresses. The ML zonal and meridional velocities $\bar{u}_*$ and $\bar{v}_*$ are then calculated. Second, for T_A, T_I, h, $\bar{u}_*$, and $\bar{v}_*$, the polynomial coefficients and the corresponding residuals are computed using weithed least-squares from a call to the routine *coepoly.f*. Third, the total ML velocity, which includes the effects of wind stress, ML temperature gradient, and ML salinity gradient, are calculated. Finally, the user is given the option either to return to the main program or to proceed in the routine. If the decision is made to proceed, a numerical solution of the mixed-layer model is produced from a call to the routine *mod-int.f*.

5.2.10 *num-rec.f*

This file is a set of routines taken from *Press et al.* (1992). The foregoing reference should be cited in any document reporting an application of the code, as these routines are used to run the code. The original routines of *Press et al.* (1992) have been subject to a very small amount of editing in order to accomodate the relatively large sizes of the matrices for the present inverse problem.

5.2.11 *opening.f*

This subroutine opens a set of output files. A number is assigned to each output file for future reference. Moreover, each output file is tagged with an extension which is the extension of the start file *start.*[tag], where [tag] is a string of 50 or less characters.

5.2.12 *P-filxx.f*

This subroutine constructs the error covariance matrix for the initial state estimate, $\mathbf{P}_0(+)$. It must be called with an argument, [nN], set equal to the order of this matrix. By definition, the diagonal elements of $\mathbf{P}_0(+)$ are the variances of the errors in the elements of $\hat{\mathbf{x}}_0(+)$, and the off-diagonal elements of $\mathbf{P}_0(+)$ are the covariances between the errors in these elements. The routine *P-filxx.f* completes three main tasks. First, it calculates the average and variance of the modern annual mean SSTs at the model grid points. Second, it sets the error variances for the initial estimates of the ML temperature equal to this variance. The error covariances for these estimates are set to zero. Finally, the subroutine assigns the error variances and error covariances for the initial estimates of the polynomial coefficients.

Note that each element of $\mathbf{P}_0(+)$ is multiplied by a factor that is prescribed in the start file, *start.*[tag]. These factors may be set to different values for different types of variable and are referred to as [fac-p0-tt] for T, [fac-p0-ta] for $c_k^{(T_A)}$, [fac-p0-ti] for $c_k^{(T_I)}$, [fac-p0-hh] for $c_k^{(h)}$, [fac-p0-uk] for $c_k^{(\bar{u}_*)}$, and [fac-p0-vk] for $c_k^{(\bar{v}_*)}$.

5.2.13 *QQxxxxx.f*

This subroutine constructs the error covariance matrix for the model equations (their finite-difference forms). This matrix, $\mathbf{Q}$, is assumed to be diagonal. As a result, it reduces to a vector in the code, with a dimension equal to the total number of model equations (their finite-difference forms). The routine *QQxxxxx.f* is called with an integer argument, [nN], which must be equal to the dimension of $\mathbf{Q}$. It performs the following main tasks. First, it sets the error variance for the T-equations (at both interior and boundary points) proportional to the square of the spatial average of the annual mean modern SSTs at the model grid points which are obtained from *WOA* (2013). This spatial average is computed previously in the routine *P-filxx.f*. Second, the routine *QQxxxxx.f* sets the error variances for the polynomial coefficient equations proportional to the square of the coefficients estimated from the modern observations. These coefficients are computed

previously in the routine *mod-sta.f*.

Note that the each element of **Q** is multiplied by a factor that is prescribed in the start file, *start.*[tag]. These factors may be set equal to different values for the equations for different variables. They are called [fac-q-tt] for the equation for T (at both interior and boundary points), [fac-q-ta] for the equation for $c_k^{(T_A)}$, [fac-q-ti] for the equation for $c_k^{(T_I)}$, [fac-q-hh] for the equation for $c_k^{(h)}$, [fac-q-uk] for the equation for $c_k^{(\bar{u}_*)}$, and [fac-q-vk] for the equation for $c_k^{(\bar{v}_*)}$. Finally, the routine *QQxxxxx.f* specifies the error variances for all the equations in **Q**.

5.2.14 *reading.f*

This file reads different data sets: the zonal and meridional wind stresses from *Risien and Chelton* (2008), the sediment SST records (section 4.1), the annual mean SSTs and their standard errors from *WOA* (2013), the annual mean salinities from *WOA* (2013), and the monthly mean ML depths from *Monterey and Levitus* (1997). The routine should be called with one argument, [c4], a 4-character string that will select between these different options. The routine calculates the fields of wind stresses, sea surface temperature, sea surface salinity, and ML depth on the model grid using averaging. The error in the gridded field of SST is determined by error propagation from the standard errors reported in *WOA* (2013), neglecting error correlation.

5.2.15 *selxxxx.f*

This subroutine returns the sediment SST record(s) that is (are) used for the inversion. It must be called with an integer argument, [n], which defines the number of records to be used in the inversion (here is an example where the code is probably in need of increased flexibility, by allowing the user to choose specific core locations to be used in the inversion). For each record, the subroutine *selxxxx.f* performs the following main tasks: it determines the corresponding longitude and latitude indices on the model grid, it records the number of SST values, it calculates annual mean SSTs by averaging values

for the 'cold' and 'warm' seasons, and it computes the error in the annual mean SSTs by error propagation (neglecting error covariances).

5.2.16 *setting.f*

This subroutine sets up the model grid (latitudes and longitudes), assigns indices to model grid points, and calculates parameters that are used for the evaluation of partial derivatives in $\partial\mathbf{f}/\partial\mathbf{x}$.

5.2.17 *smoothe.f*

This subroutine applies the Linearized Smoother to combine the Linearized Kalman Filter solution with posterior observations. It calculates the transpose of the matrix of partial derivatives, $\partial\mathbf{f}/\partial\mathbf{x}$, and then proceeds to the algorithm detailed in section 4.3.5. In contrast to the routines for the Kalman filters, *fil-lkf.f* and *fil-ekf.f*, the time loop in the routine *smoothe.f* is backward, starting from a future time defined by [itot-fs]. Within the loop, the prior and posterior state estimates obtained from the LKF, $\hat{\mathbf{x}}_i(-)$ and $\hat{\mathbf{x}}_i(+)$, respectively, as well as elements of the error covariance matrix for the posterior estimate, $\mathbf{P}_i(+)$, are read at each discrete time [it] of the loop. The routine *smoothe.f* performs the various tasks of the LS and periodically writes out results from multiple calls to *writing.f*.

5.2.18 *stringx.f*

This function returns a 8-character string, [strx()], for a state variable defined in $\mathbf{x}$. This character string is constructed from the three arguments for this function: [c2] defines the physical nature of the variable, [i] is a longitude index, and [j] is a latitude index.

5.2.19 *sv-to-x.f*

This subroutine constructs the state vector $\mathbf{x}$ from the state variables. It must be called with 2 arguments: [xx] is the state vector to be constructed and [nN] is the dimension of this vector.

5.2.20 *uuxxxxx*

This function returns the value of the ML zonal velocity at a given location of the model grid. It should be called with 4 arguments: [i] is the longitude index of the velocity, [j] is the latitude index of the velocity, [i-E] should be set to 1 (0) if the Ekman contribution to the velocity is to be considered (disregarded), [i-T] should be set to 1 (0) if the thermal contribution to the velocity is to the considered (disregarded), and [i-S] should be set to 1 (0) if the saline contribution to the velocity is to the considered (disregarded).

5.2.21 *vvxxxxx*

This function returns the value of the ML meridional velocity at a given location of the model grid. It should be called with 4 arguments: [i] is the longitude index of the velocity, [j] is the latitude index of the velocity, [i-E] should be set to 1 (0) if the Ekman contribution to the velocity is to be considered (disregarded), [i-T] should be set to 1 (0) if the thermal contribution to the velocity is to the considered (disregarded), and [i-S] should be set to 1 (0) if the saline contribution to the velocity is to the considered (disregarded).

5.2.22 *w-ixxxx.f*

This subroutine returns the vertical interior velocities, w_I, at all interior points of the model grid using a finite-difference approximation of the continuity equation (15).

5.2.23 *writing.f*

This subroutine writes code results in the output files. It is called with a list of 3 arguments: [c14] defines the physical nature of the variable to be written, [ifile] is the number of the output file, and [it] is a time index. The general structure of the routine *writing.f* consists in a set of tests on [c14].

5.2.24 *wr-xfil.f*

This subroutine writes or reads the posterior state estimates, $\hat{\mathbf{x}}_i(+)$, and their error covariance matrices, $\mathbf{P}_i(+)$, which are derived from the LKF and used by the LS. It must be called with 3 arguments: [c5-wr] is used to instruct reading or writing, [it] corresponds to the time index i of $\hat{\mathbf{x}}_i(+)$ and $\mathbf{P}_i(+)$, and [Nn] specifies the dimension (order) of $\hat{\mathbf{x}}_i(-)$ ($\mathbf{P}_i(+)$). Note that only the elements along and below the diagonal of $\mathbf{P}_i(+)$ are written and read. After reading the matrix $\mathbf{P}_i(+)$, the elements above the diagonal of the matrix are obtained from the elements below the diagonal.

5.2.25 *wr-xmxx.f*

This subroutine writes or reads the prior state estimates, $\hat{\mathbf{x}}_i(-)$, that are derived from the LKF and used by the LS. It must be called with 3 arguments: [c5-wr] is used to instruct reading or writing, [it] corresponds to the time index i of $\hat{\mathbf{x}}_i(-)$, and [Nn] specifies the dimension of $\hat{\mathbf{x}}_i(-)$.

5.2.26 *x-to-sv.f*

This subroutine extracts the state variables and their errors from, respectively, an estimate of the state vector and its error covariance matrix. It must be called with 3 arguments: [xx] is the vector from which the state variables must be extracted, [Px] is the error covariance matrix from which the errors in these variables should be extracted, and [nN] is the dimension (order) of this vector (matrix). The routine *x-to-sv.f* also calculates, from the extracted polynomial coefficients, the fields of (i) apparent atmospheric temperature, (ii) interior temperature, (iii) ML depth, (iv) ML zonal velocity $\bar{u}$, and (v) ML meridional velocity $\bar{v}$.

5.2.27 *zzRRHob.f*

This subroutine constructs (i) the vector of measurements ($\mathbf{z}_i$), (ii) the error covariance matrix for the measurements ($\mathbf{R}_i$), and (iii) the measurement matrix ($\mathbf{H}_i$). It is called with two arguments: [time] is the time of the measurements and [np] is the number of measurements. The first is an input to the routine and the second is an output from the routine. Note that the measurements include both SST estimates from the sediment records as well as modern observational estimates of SST and other quantities.

5.3 Common File

The main program and the routines share a common set of variables that are declared in the file *commonvar.f*. This is done through the statement **include 'commonvar.f'**. which is placed at the beginning of the main program and of the routines. Thus, when a change is made to *commonvar.f*, it is automatically transmitted to the main program and to the routines where the statement **include 'commonvar.f'** appears. The variables declared in *commonvar.f* are parameters (quantities that are fixed during the execution of the program) and actual variables. A definition of each variable that is declared in the file *commonvar.f* is provided in this file. Both the type and the dimension of the variables are declared, and the actual variables are put in 'common blocks'.

5.4 Makefile

The file *makefile* is used to compile the code. It links the main program with the routines, and produces object files from which the code is executed. Everytime a change is made to the code, the code should be recompiled using *makefile* in order to ensure that this change will be considered in a future execution of the program. The first line of *makefile* is the name of the command for running the FORTRAN compiler that is at the user's disposal. The second line is a list of options for the compilation of the main program and of the routines. Among these options is the precision of the arithmetic operations to be carried out by the program. The calculations in the code are carried out with double precision.

From the author's experience, changing the content of a *makefile* requires great caution. For example, the *makefile* may include symbols, such as those generated from the Tab key, that may not show up on the monitor with some text editors but that may be needed for a successful compilation. For this reason, it is probably advisable to always save a copy of the *makefile* before making any change to this file.

6 Preparing an Inversion & Running the Program

6.1 Preparing an Inversion

The computer code can be used to conduct filtering and (or) smoothing experiments. In the sequel, either type of experiment is referred to as an 'inversion'. The number and type of operations that must be completed in order to prepare an inversion with the computer code obviously depend on the user's particular investigation. Nevertheless, the following set operations are anticipated to be generally needed:

1. The user should edit the start file in order to specify various aspects of the inversion. Thus, the type of filter (LKF or EKF) to be applied must be selected via the variable [c3-KF], the decision to write out or not LKF results for use by the LS must be stated via [i-Store], the factors for the prior error covariance matrix must be specified via the variables [fac-p0-**], and the factors for the model error covariance matrix must be prescribed via [fac-q-**]. Importantly, if the decision is made to write out LKF results, then the following sub-directories should be created in the code directory before running the code: (1) Store/Xm, where the prior state error estimates, $\hat{\mathbf{x}}_i(-)$, will be written and read, (2) Store/X-fil, where the posterior state error estimates, $\hat{\mathbf{x}}_i(+)$, will be written and read, and (3) Store/P-fil, where elements along and below the error covariance matrix for the posterior state estimates, $\mathbf{P}_i(+)$, will be written and read. It is advisable that the user verifies that he (she) has the storage capacity available to produce the files in these three sub-directories. The size of these files is determined by the dimension of the state vector, [ndim], and their number is determined by the number of iterations that is set in the routine *fil-lkf.f*, [itot-fs].

2. The geographic domain of investigation should be defined by the user, depending on the location of the SST records, the nature of the research question, and the computational resources available. The user can define the domain by modifying some of the variables declared in *commonvar.f* and by editing the routine *setting.f*. The variables in *commonvar.f* that would need to be modified are those which define the

dimension of arrays ([idim],[jdim],[ndim]) and those which define the lateral boundaries of the domain ([lon-W],[lon-E],[lat-S],[lat-N]). Other variables may also need to be changed, depending on the particular investigation. For example, the user may want to experiment a different number of terms for the polynomial functions (29), in which case the value of [ncoedim] will also need to be changed. To accomodate a new geographic domain, the variables to be changed in *setting.f* include in particular the grid point indices ([ipt]), the longitude indices ([iE],[iW]), the latitude indices ([jS],[jN]), as well as the indices for the corner points ([i-cor],[j-cor]).

3. The SST records to combine with the advective ML model should be available in one or several external files. These data files will be opened, read, and closed in the routine *opening.f*, which is called by the main program, *main.f*. Clearly, the data files must be structured in a way that is consistent with the reading statements in this routine. Alternately, the reading statements in *opening.f* could be altered to comply with a different structure of the data files. The routine *selxxxx.f* selects the SST records used for the inversion, averages seasonal SST values, and calculates the uncertainties in the resulting values by error propagation. Any of these operations could be modified to accomodate a new dataset, if needed.

4. In the same vein, the user could mofidy the routines *reading.f* and *mod-sta.f*, if a different dataset is used to constrain modern observational estimates of SST, sea surface salinity, ML depth, zonal wind stress, and (or) meridional wind stress. The routine *coepoly.f* could also be changed to consider a different approach than the use of polynomial functions to approximate the spatial fields (29).

5. The advective ML model should be modified if the user desires to experiment a different model. For example, the functions *uuxxxx.f* and *vvxxxx.f* could be changed to consider a different calculation of the ML zonal and meridional velocities. The method of solution and (or) the open boundary conditions could be also be modified, which would require editing the routine *mod-int.f*. Note that if a finite-difference equation is changed in *mod-int.f*, its partial derivatives with respect to the state variables that are included in $\partial\mathbf{f}/\partial\mathbf{x}$ will also change. If this is the case, the new

expressions for the partial derivatives should be evaluated and implemented in the routine *df-dxxx.f*.

6. The beginning and duration of the inversion should be set up. The beginning of the inversion (expressed in calendar year) is determined by the value of [time-start], which is assigned in *commonvar.f*. The duration of the inversion is determined by the value of [itot-fs], which is assigned in *main.f*.

7. The user may also need to modify aspects of the LKF or EKF, depending on the particular investigation. For example, the estimate of the initial state, $\hat{\mathbf{x}}_0(+)$, and its error covariance matrix, $\mathbf{P}_0(+)$, must incorporate prior knowledge about the state and its uncertainty at the initial time of the filtering experiment. The error covariance matrix for the model equations, *QQxxxx.f*, can be changed to consider the available constraints on the error statistics of these equations. A different algorithm could be used for the filters in *fil-lkf.f* and *fil-ekf.f*. For example, the more computationally efficient formula for the prior uncertainty, $\mathbf{P}_i(+) = [\mathbf{I} - \mathbf{K}_i\mathbf{H}_i]\mathbf{P}_i(-)$, could be coded, square-root filtering, and (or) filtering based in information matrices could be implemented (*Anderson and Moore*, 1979).

8. Likewise, the user might find it advantageous to code another fixed-interval smoother. As already mentioned in this document, the smoother being coded in *smoothe.f* is particularly efficient for the case where the dimension of the measurement vectors, $\mathbf{z}_i$, is much smaller than the dimension of the state vector, $\mathbf{x}_i$. If such is not the case for the user's investigation, a different algorithm could be developed. The user might also want to calculate the estimate of the model errors, $\mathbf{w}_i$, as well as their covariance matrix, $\mathbf{Q}_i$. None of these two quantities are computed in the present code, although recursive formulae to compute them have also available (see *Bryson and Ho* (1975); p. 392).

6.2 Running the Program

Once the file *start.*[tag] is produced and the code is modified to accomodate the user's particular investigation, the code should be ready for execution. The code has been run by this author on a Niveus 5200 workstation (dual Intel Xeon E5-2643, 4C, 3.3 GHz, 1600 MHz RAM, 64 GB, DDR3-1600 ECC (8x8 GB)), which relies on the CentOS operating system (a Linux distribution). In order to execute the program, the user should enter the following command,

```
> ./main
```

After entering the command, the following statement appears on the user's monitor or on any other external unit defined by the user in *main.f*:

```
- - - - - - - - - - - - - - - - - - - - - - - - -
Enter the extension of the START file
- - - - - - - - - - - - - - - - - - - - - - - - -
```

Here, the user should provide the extension of the start file, *start.*[tag], which he (she) would have produced to prepare the inversion. The execution of the program should then start. The user is informed about the progress of the inversion through the discrete times of the filtering and (or) smoothing calculations, which stream on the monitor or external unit. At the end of the program, the following statement appears on the monitor or external unit:

```
- - - - - - - - - - - - - - - - - - - - - - -
Normal exit: file extension: [tag]
- - - - - - - - - - - - - - - - - - - - - - -
```

At this stage, the output files with extension [tag] and opened in *opening.f*, as well as the other output files with extension [r] and opened in other routines, have been produced.

7 Acknowledgements

This code has been written in the framework of a research project entitled "Kalman filtering and smoothing of sediment records from the Atlantic Ocean from the past 20 kyrs" and funded by the U.S. National Science Foundation. The author also expresses his gratitude to Katherine Allen, Daniel Amrhein, Brian Farrell, Geoffrey Gebbie, Lloyd Keigwin, Delia Oppo, Eli Tziperman, and Carl Wunsch for useful discussions over the course of this project. Sarah Shipley worked as a Guest Student on several aspects of this project.

8 Appendices

8.1 Appendix A: Modern Observational Estimates of $T_A, T_I, S, h, \boldsymbol{\tau}_s$

The apparent atmospheric temperatures, T_A, are obtained from the annual mean ('statistical means', 'averaged decades') SSTs ($z = 0$ m) with 1°×1° horizontal resolution which are available in the World Ocean Atlas (*WOA*, 2013). The annual mean SSTs of the World Ocean Atlas are averaged in 2°×2° cells centered at the T-carrier points of the model grid to produce the modern values of T_A. The interior temperatures, T_I, are derived from the same procedure, except that these temperatures are reduced by 0.5°C, consistent with our criterion for ML depth (see below). The values of surface salinity, S, are obtained from the annual mean ('statistical means', 'averaged decades') surface salinities ($z = 0$ m) with 1°×1° horizontal resolution which are reported in *WOA* (2013). The annual mean salinities of the World Ocean Atlas are averaged in 2°×2° cells centered at the S-carrier points of the model grid to produce the modern values of S. The ML depths, h, are obtained from a climatology of monthly mean ML depths based on a 0.5°C-potential temperature criterion and available with 1°×1° resolution (*Monterey and Levitus*, 1997). A distribution of annual mean ML depth with the same resolution is computed by avegaring the monthly climatological values. The annual mean ML depths are then averaged in 2°×2° cells centered at the h-carrier points to produce the modern values of h. Finally, the surface wind stresses are derived from the Scatterometer Climatology of Ocean Winds, SCOW (*Risien and Chelton*, 2008). The monthly mean zonal and meridional wind stresses, available at 1/4°×1/4° resolution, are averaged to produce annual means. The annual mean values of zonal (meridional) stress are then averaged in 2°×2° cells centered at the $\bar{v}$- ($\bar{u}$-) carrier points.

8.2 Appendix B: Estimation of Polynomial Coefficients

Consider for the sake of illustration the estimation of $c_k^{(T_A)}$, with $k = 1, 2, \cdots, K$. Equations (29) lead to systems of linear albegraic equations, one system for each variable and one equation for each pair (λ_c, ϕ_c). The system for the variable T_A can be written as

$$\mathbf{Ec} + \mathbf{n} = \mathbf{y}, \tag{B1}$$

where $\mathbf{c} = (c_1^{(T_A)}, c_2^{(T_A)}, \cdots, c_K^{(T_A)})'$, $\mathbf{E}$ is a coefficient matrix, $\mathbf{y}$ is a vector of modern data, and $\mathbf{n}$ is a vector that includes the errors in these data. The data in this case are observational estimates of the apparent atmospheric temperature. They are obtained by averaging in the $2°\times2°$ model grid cells the modern annual mean SSTs with $1°\times1°$ horizontal resolution reported in *WOA* (2013) (Appendix A). The errors in these data are calculated by propagating the standard errors in the annual mean SSTs (*WOA*, 2013) contributing to the cell averages, neglecting error correlation. The squares of these errors are included along the diagonal of a square matrix, $\mathbf{R}_{nn}$. The off-diagonal elements of $\mathbf{R}_{nn}$ are set to zero. An estimate of $\mathbf{c}$ that minimizes the sum of weighted squared errors, $\mathbf{n}'\mathbf{R}_{nn}^{-1}\mathbf{n}$, is then sought. This weighted least-squares estimate and its uncertainty are given by (e.g., *Wunsch*, 2006)

$$\hat{\mathbf{c}} = (\mathbf{E}'\mathbf{R}_{nn}^{-1}\mathbf{E})^{-1}\mathbf{E}'\mathbf{R}_{nn}^{-1}\mathbf{y}, \tag{B2a}$$

$$\mathbf{P} = (\mathbf{E}'\mathbf{R}_{nn}^{-1}\mathbf{E})^{-1}. \tag{B2b}$$

The other coefficients, $c_k^{(T_I)}, c_k^{(h)}, c_k^{(\bar{u}_*)}, c_k^{(\bar{v}_*)}$ are estimated along the same lines. For $c_k^{(T_I)}$, the data in $\mathbf{y}$ are as described in appendix A and their errors represented in $\mathbf{R}_{nn}$ (assumed diagonal) are the same as for $c_k^{(T_A)}$. For $c_k^{(h)}$, the data in $\mathbf{y}$ are as described in appendix A and their errors represented in $\mathbf{R}_{nn}$ (assumed diagonal) are assumed to be 10 m. Finally, for $c_k^{(\bar{u}_*)}$ and $c_k^{(\bar{v}_*)}$, the data in $\mathbf{y}$ are the zonal and meridional velocity components, $\bar{u}_*$ and $\bar{v}_*$, computed from the wind stress and salinity data described in appendix A, using the numerical scheme detailed in section 4.2.6. Their errors represented in $\mathbf{R}_{nn}$ (assumed diagonal) are set equal to 0.1 cm s^{-1}.

8.3 Appendix C: Matrix of partial derivatives $\partial \mathbf{f}/\partial \mathbf{x}$

The construction of the matrix of partial derivatives of the model equations with respect to the state variables, $\partial \mathbf{f}/\partial \mathbf{x}$, is probably the most delicate aspect of EKF and LKF. The difference equations of the model are (i) the equation for ML temperature at the interior points, (ii) the equation for ML temperature at the boundary points, and (iii) the equations for the polynomial coefficients $(c_k^{(T_A)}, c_k^{(T_I)}, c_k^{(h)}, c_k^{(\bar{u}_*)}, c_k^{(\bar{v}_*)})$. In this appendix, we list the partial derivatives of each of these equations with respect to the variables defined in the state vector (31). To lighten notation, the overbar above the velocities are dropped.

Derivatives of ML temperature equation at interior points

The difference equation for ML temperature at interior point (i, j) is written as (19)

$$\begin{aligned} T_{i,j}^{n+1} = T_{i,j}^n \quad & - \quad \frac{\Delta t}{r\cos\phi_j \Delta\lambda}\left(\frac{u_{*,\mathrm{i+1/2,j}} + |u_{*,\mathrm{i+1/2,j}}|}{2} T_{i,j}^n + \frac{u_{*,\mathrm{i+1/2,j}} - |u_{*,\mathrm{i+1/2,j}}|}{2} T_{i+1,j}^n\right) \\ & + \quad \frac{\Delta t}{r\cos\phi_j \Delta\lambda}\left(\frac{u_{*,\mathrm{i\text{-}1/2,j}} + |u_{*,\mathrm{i\text{-}1/2,j}}|}{2} T_{i-1,j}^n + \frac{u_{*,\mathrm{i\text{-}1/2,j}} - |u_{*,\mathrm{i\text{-}1/2,j}}|}{2} T_{i,j}^n\right) \\ & - \quad \frac{\Delta t}{r\Delta\phi}\left(\frac{v_{*,\mathrm{i,j+1/2}} + |v_{*,\mathrm{i,j+1/2}}|}{2} T_{i,j}^n + \frac{v_{*,\mathrm{i,j+1/2}} - |v_{*,\mathrm{i,j+1/2}}|}{2} T_{i,j+1}^n\right) \\ & + \quad \frac{\Delta t}{r\Delta\phi}\left(\frac{v_{*,\mathrm{i,j\text{-}1/2}} + |v_{*,\mathrm{i,j\text{-}1/2}}|}{2} T_{i,j-1}^n + \frac{v_{*,\mathrm{i,j\text{-}1/2}} - |v_{*,\mathrm{i,j\text{-}1/2}}|}{2} T_{i,j}^n\right) \\ & + \quad \frac{\Delta t}{r}\left(\frac{u_{*,\mathrm{i+1/2,j}} - u_{*,\mathrm{i\text{-}1/2,j}}}{\cos\phi_j \Delta\lambda} + \frac{v_{*,\mathrm{i,j+1/2}} - v_{*,\mathrm{i,j\text{-}1/2}}}{\Delta\phi}\right) T_{i,j}^n \\ & + \quad \Delta t \frac{w_A}{h_{i,j}}\left(T_{A,i,j}^n - T_{i,j}^n\right) + \Delta t \frac{w_{I,i,j}}{h_{i,j}}\left(T_{I,i,j}^n - T_{i,j}^n\right), \end{aligned} \tag{C1}$$

where

$$w_{I,i,j} = \frac{u_{\mathrm{i+1/2,j}}\bar{h}_{\mathrm{i+1/2,j}} - u_{\mathrm{i\text{-}1/2,j}}\bar{h}_{\mathrm{i\text{-}1/2,j}}}{r\cos\phi_j\Delta\lambda} + \frac{v_{\mathrm{i,j+1/2}}\bar{h}_{\mathrm{i,j+1/2}}\cos\phi_{\mathrm{j+1/2}} - v_{\mathrm{i,j\text{-}1/2}}\bar{h}_{\mathrm{i,j\text{-}1/2}}\cos\phi_{\mathrm{j\text{-}1/2}}}{r\Delta\sin\phi}, \tag{C2}$$

with $\Delta\sin\phi = \sin\phi_{\mathrm{j+1/2}} - \sin\phi_{\mathrm{j\text{-}1/2}}$. In (C1–C2), the velocities (u_*, v_*, W_I) and the ML depths are implicitly defined at the time level n (w_A is considered constant). The velocities (u_*, v_*) include the Ekman and saline contributions, and are derived from the polynomial coefficients, e.g.,

$$u_{*,\mathrm{i+1/2,j}} = \sum_{k=1}^{K} c_k^{(\bar{u}_*)} \lambda_{c,\mathrm{i+1/2}}^{a_k} \phi_{c,\mathrm{j}}^{b_k} + \tilde{u}_{*,\mathrm{i+1/2,j}}, \tag{C3a}$$

$$v_{*,\mathrm{i,j+1/2}} = \sum_{k=1}^{K} c_k^{(\bar{v}_*)} \lambda_{c,\mathrm{i}}^{a_k} \phi_{c,\mathrm{j+1/2}}^{b_k} + \tilde{v}_{*,\mathrm{i,j+1/2}}. \tag{C3b}$$

The velocities (u, v) are the sum of all contributions, i.e., the Ekman, saline, and thermal contributions:

$$u_{\mathrm{i+1/2,j}} = u_{*,\mathrm{i+1/2,j}} + u_{T,\mathrm{i+1/2,j}}, \tag{C4a}$$

$$v_{\mathrm{i,j+1/2}} = v_{*,\mathrm{i,j+1/2}} + v_{T,\mathrm{i,j+1/2}}. \tag{C4b}$$

In these equations, the thermal contributions can be expressed as

$$u_{T,\mathrm{i+1/2,j}} = \gamma_j \left(h_{i,j} + h_{i+1,j}\right)\left(T_{i,j+1} + T_{i+1,j+1} - T_{i,j-1} - T_{i+1,j-1}\right), \tag{C5a}$$

$$v_{T,\mathrm{i,j+1/2}} = \delta_j \left(h_{i,j} + h_{i,j+1}\right)\left(T_{i+1,j+1} + T_{i+1,j} - T_{i-1,j+1} - T_{i-1,j}\right), \tag{C5b}$$

where

$$\gamma_j = \frac{\alpha g}{16\Omega r\left(\cos\phi_{j+1} - \cos\phi_{j-1}\right)}, \tag{C6a}$$

$$\delta_j = \frac{\alpha g}{16\Omega r \sin(2\phi_{\mathrm{j+1/2}})\Delta\lambda}. \tag{C6b}$$

In order to evaluate the partial derivatives, equation (C1) is re-written as

$$T_{i,j}^{n+1} = f_{T,i,j}\left(T_{1,1}, \cdots, c_1^{(T_A)}, \cdots, c_1^{(T_I)}, \cdots, c_1^{(h)}, \cdots, c_1^{(\bar{u}_*)}, \cdots, c_1^{(\bar{v}_*)}, \cdots\right), \tag{C7}$$

where the arguments of the function $f_{T,i,j}$, all implicitly defined at time level n, are the state variables defined in (31). The partial derivatives of $f_{T,i,j}$ that do not vanish are listed below (superscript n omitted). The partial derivative of $f_{T,i,j}$ with respect to $T_{i-1,j-1}^n$ is

$$\begin{aligned}\frac{\partial f_{T,i,j}}{\partial T_{i-1,j-1}} &= \frac{\Delta t}{h_{i,j}}\left(T_{I,i,j} - T_{i,j}\right)\frac{\bar{h}_{\mathrm{i\text{-}1/2,j}}}{r\cos\phi_j\Delta\lambda}\gamma_j\left(h_{i-1,j} + h_{i,j}\right) \\ &+ \frac{\Delta t}{h_{i,j}}\left(T_{I,i,j} - T_{i,j}\right)\frac{\bar{h}_{\mathrm{i,j\text{-}1/2}}\cos\phi_{\mathrm{j\text{-}1/2}}}{r\Delta\sin\phi}\delta_{j-1}\left(h_{i,j-1} + h_{i,j}\right).\end{aligned} \tag{C8}$$

The partial derivative of $f_{T,i,j}$ with respect to $T_{i-1,j}^n$ is

$$\begin{aligned}\frac{\partial f_{T,i,j}}{\partial T_{i-1,j}} &= \frac{\Delta t}{r\cos\phi_j\Delta\lambda}\frac{u_{*,\mathrm{i\text{-}1/2,j}} + |u_{*,\mathrm{i\text{-}1/2,j}}|}{2} \\ &- \frac{\Delta t}{h_{i,j}}\left(T_{I,i,j} - T_{i,j}\right)\frac{\bar{h}_{\mathrm{i,j+1/2}}\cos\phi_{\mathrm{j+1/2}}}{r\Delta\sin\phi}\delta_j\left(h_{i,j} + h_{i,j+1}\right) \\ &+ \frac{\Delta t}{h_{i,j}}\left(T_{I,i,j} - T_{i,j}\right)\frac{\bar{h}_{\mathrm{i,j\text{-}1/2}}\cos\phi_{\mathrm{j\text{-}1/2}}}{r\Delta\sin\phi}\delta_{j-1}\left(h_{i,j-1} + h_{i,j}\right).\end{aligned} \tag{C9}$$

The partial derivative of $f_{T,i,j}$ with respect to $T_{i-1,j+1}^n$ is

$$\begin{aligned}\frac{\partial f_{T,i,j}}{\partial T_{i-1,j+1}} &= -\frac{\Delta t}{h_{i,j}}\left(T_{I,i,j} - T_{i,j}\right)\frac{\bar{h}_{\mathrm{i\text{-}1/2,j}}}{r\cos\phi_j\Delta\lambda}\gamma_j\left(h_{i-1,j} + h_{i,j}\right) \\ &- \frac{\Delta t}{h_{i,j}}\left(T_{I,i,j} - T_{i,j}\right)\frac{\bar{h}_{\mathrm{i,j+1/2}}\cos\phi_{\mathrm{j+1/2}}}{r\Delta\sin\phi}\delta_j\left(h_{i,j} + h_{i,j+1}\right).\end{aligned} \tag{C10}$$

The partial derivative of $f_{T,i,j}$ with respect to $T^n_{i,j+1}$ is

$$\begin{aligned}\frac{\partial f_{T,i,j}}{\partial T_{i,j+1}} &= -\frac{\Delta t}{r\Delta\phi}\frac{v_{*,\mathrm{i,j+1/2}}-|v_{*,\mathrm{i,j+1/2}}|}{2} \\ &+ \frac{\Delta t}{h_{i,j}}\left(T_{I,i,j}-T_{i,j}\right)\frac{\bar{h}_{\mathrm{i+1/2,j}}}{r\cos\phi_j\Delta\lambda}\gamma_j\left(h_{i,j}+h_{i+1,j}\right) \\ &- \frac{\Delta t}{h_{i,j}}\left(T_{I,i,j}-T_{i,j}\right)\frac{\bar{h}_{\mathrm{i\text{-}1/2,j}}}{r\cos\phi_j\Delta\lambda}\gamma_j\left(h_{i-1,j}+h_{i,j}\right). \end{aligned} \tag{C11}$$

The partial derivative of $f_{T,i,j}$ with respect to $T^n_{i+1,j+1}$ is

$$\begin{aligned}\frac{\partial f_{T,i,j}}{\partial T_{i+1,j+1}} &= \frac{\Delta t}{h_{i,j}}\left(T_{I,i,j}-T_{i,j}\right)\frac{\bar{h}_{\mathrm{i+1/2,j}}}{r\cos\phi_j\Delta\lambda}\gamma_j\left(h_{i,j}+h_{i+1,j}\right) \\ &+ \frac{\Delta t}{h_{i,j}}\left(T_{I,i,j}-T_{i,j}\right)\frac{\bar{h}_{\mathrm{i,j+1/2}}\cos\phi_{\mathrm{j+1/2}}}{r\Delta\sin\phi}\delta_j\left(h_{i,j}+h_{i,j+1}\right). \end{aligned} \tag{C12}$$

The partial derivative of $f_{T,i,j}$ with respect to $T^n_{i+1,j}$ is

$$\begin{aligned}\frac{\partial f_{T,i,j}}{\partial T_{i+1,j}} &= -\frac{\Delta t}{r\cos\phi_j\Delta\lambda}\frac{u_{*,\mathrm{i+1/2,j}}-|u_{*,\mathrm{i+1/2,j}}|}{2} \\ &+ \frac{\Delta t}{h_{i,j}}\left(T_{I,i,j}-T_{i,j}\right)\frac{\bar{h}_{\mathrm{i,j+1/2}}\cos\phi_{\mathrm{j+1/2}}}{r\Delta\sin\phi}\delta_j\left(h_{i,j}+h_{i,j+1}\right) \\ &- \frac{\Delta t}{h_{i,j}}\left(T_{I,i,j}-T_{i,j}\right)\frac{\bar{h}_{\mathrm{i,j\text{-}1/2}}\cos\phi_{\mathrm{j\text{-}1/2}}}{r\Delta\sin\phi}\delta_{j-1}\left(h_{i,j-1}+h_{i,j}\right). \end{aligned} \tag{C13}$$

The partial derivative of $f_{T,i,j}$ with respect to $T^n_{i+1,j-1}$ is

$$\begin{aligned}\frac{\partial f_{T,i,j}}{\partial T_{i+1,j-1}} &= -\frac{\Delta t}{h_{i,j}}\left(T_{I,i,j}-T_{i,j}\right)\frac{\bar{h}_{\mathrm{i+1/2,j}}}{r\cos\phi_j\Delta\lambda}\gamma_j\left(h_{i,j}+h_{i+1,j}\right) \\ &- \frac{\Delta t}{h_{i,j}}\left(T_{I,i,j}-T_{i,j}\right)\frac{\bar{h}_{\mathrm{i,j\text{-}1/2}}\cos\phi_{\mathrm{j\text{-}1/2}}}{r\Delta\sin\phi}\delta_{j-1}\left(h_{i,j-1}+h_{i,j}\right). \end{aligned} \tag{C14}$$

The partial derivative of $f_{T,i,j}$ with respect to $T^n_{i,j-1}$ is

$$\begin{aligned}\frac{\partial f_{T,i,j}}{\partial T_{i,j-1}} &= \frac{\Delta t}{r\Delta\phi}\frac{v_{*,\mathrm{i,j\text{-}1/2}}+|v_{*,\mathrm{i,j\text{-}1/2}}|}{2} \\ &- \frac{\Delta t}{h_{i,j}}\left(T_{I,i,j}-T_{i,j}\right)\frac{\bar{h}_{\mathrm{i+1/2,j}}}{r\cos\phi_j\Delta\lambda}\gamma_j\left(h_{i,j}+h_{i+1,j}\right) \\ &+ \frac{\Delta t}{h_{i,j}}\left(T_{I,i,j}-T_{i,j}\right)\frac{\bar{h}_{\mathrm{i\text{-}1/2,j}}}{r\cos\phi_j\Delta\lambda}\gamma_j\left(h_{i-1,j}+h_{i,j}\right). \end{aligned} \tag{C15}$$

The partial derivative of $f_{T,i,j}$ with respect to $T^n_{i,j}$ is

$$\begin{aligned}\frac{\partial f_{T,i,j}}{\partial T_{i,j}} = 1 &- \frac{\Delta t}{r\cos\phi_j\Delta\lambda}\left(\frac{u_{*,\mathrm{i+1/2,j}}+|u_{*,\mathrm{i+1/2,j}}|}{2}-\frac{u_{*,\mathrm{i\text{-}1/2,j}}-|u_{*,\mathrm{i\text{-}1/2,j}}|}{2}\right) \\ &- \frac{\Delta t}{r\Delta\phi}\left(\frac{v_{*,\mathrm{i,j+1/2}}+|v_{*,\mathrm{i,j+1/2}}|}{2}-\frac{v_{*,\mathrm{i,j\text{-}1/2}}-|v_{*,\mathrm{i,j\text{-}1/2}}|}{2}\right) \end{aligned}$$

$$+ \quad \frac{\Delta t}{r}\left(\frac{u_{*,\mathrm{i+1/2,j}}-u_{*,\mathrm{i\text{-}1/2,j}}}{\cos\phi_j\Delta\lambda}+\frac{v_{*,\mathrm{i,j+1/2}}-v_{*,\mathrm{i,j\text{-}1/2}}}{\Delta\phi}\right)$$
$$- \quad \frac{\Delta t}{h_{i,j}}\left(w_A+w_{I,i,j}\right). \tag{C16}$$

The partial derivative of $f_{T,i,j}$ with respect to $c_k^{(T_A)(n)}$ and $c_k^{(T_I)(n)}$ are given by, respectively,

$$\frac{\partial f_{T,i,j}}{\partial c_k^{(T_A)}} = \Delta t\frac{w_A}{h_{i,j}}\lambda_{c,i}^{a_k}\phi_{c,j}^{b_k}, \tag{C17a}$$
$$\frac{\partial f_{T,i,j}}{\partial c_k^{(T_I)}} = \Delta t\frac{w_{I,i,j}}{h_{i,j}}\lambda_{c,i}^{a_k}\phi_{c,j}^{b_k}. \tag{C17b}$$

The partial derivative of $f_{T,i,j}$ with respect to $c_k^{(h)(n)}$ is computed from

$$\begin{aligned}\frac{\partial f_{T,i,j}}{\partial c_k^{(h)}} = &- \Delta t\frac{w_A}{h_{i,j}^2}\left(T_{A,i,j}-T_{i,j}\right)\lambda_{c,i}^{a_k}\phi_{c,j}^{b_k}\\ &- \Delta t\frac{w_{I,i,j}}{h_{i,j}^2}\left(T_{I,i,j}-T_{i,j}\right)\lambda_{c,i}^{a_k}\phi_{c,j}^{b_k}\\ &+ \frac{\Delta t}{h_{i,j}}\left(T_{I,i,j}-T_{i,j}\right)\frac{\partial w_{I,i,j}}{\partial c_k^{(h)}}.\end{aligned} \tag{C18}$$

Here $\partial w_{I,i,j}/\partial c_k^{(h)}$ is obtained from

$$\frac{\partial w_{I,i,j}}{\partial c_k^{(h)}} = \frac{\partial w_{I,i,j}}{\partial c_k^{(h)}}|_1 + \frac{\partial w_{I,i,j}}{\partial c_k^{(h)}}|_2, \tag{C19}$$

where

$$\begin{aligned}\frac{\partial w_{I,i,j}}{\partial c_k^{(h)}}|_1 = &\frac{1}{2r\cos\phi_j\Delta\lambda}\left(u_{\mathrm{i+1/2,j}}+u_{\mathrm{T,i+1/2,j}}\right)\left(\lambda_{c,i}^{a_k}+\lambda_{c,i+1}^{a_k}\right)\phi_{c,j}^{b_k}\\ &- \frac{1}{2r\cos\phi_j\Delta\lambda}\left(u_{\mathrm{i\text{-}1/2,j}}+u_{\mathrm{T,i\text{-}1/2,j}}\right)\left(\lambda_{c,i-1}^{a_k}+\lambda_{c,i}^{a_k}\right)\phi_{c,j}^{b_k}\end{aligned} \tag{C20}$$

and

$$\begin{aligned}\frac{\partial w_{I,i,j}}{\partial c_k^{(h)}}|_2 = &\frac{\cos\phi_{\mathrm{j+1/2}}}{2r\Delta\sin\phi}\left(v_{\mathrm{i,j+1/2}}+v_{\mathrm{T,i,j+1/2}}\right)\left(\phi_{c,j}^{b_k}+\phi_{c,j+1}^{b_k}\right)\lambda_{c,i}^{a_k}\\ &- \frac{\cos\phi_{\mathrm{j\text{-}1/2}}}{2r\Delta\sin\phi}\left(v_{\mathrm{i,j\text{-}1/2}}+v_{\mathrm{T,i,j\text{-}1/2}}\right)\left(\phi_{c,j-1}^{b_k}+\phi_{c,j}^{b_k}\right)\lambda_{c,i}^{a_k}.\end{aligned} \tag{C21}$$

The partial derivative of $f_{T,i,j}$ with respect to $c_k^{(u_*)(n)}$ and $c_k^{(v_*)(n)}$ are evaluated using the following formula for the differentiation of the absolute value of a generic function $f(x)$,

$$\frac{\mathrm{d}|f(x)|}{\mathrm{d}x} = \frac{f(x)}{|f(x)|}\frac{\mathrm{d}f(x)}{\mathrm{d}x} = \mathrm{s}\left[f(x)\right]\frac{\mathrm{d}f(x)}{\mathrm{d}x}, \tag{C22}$$

assuming $f(x) \neq 0$ and where $\mathrm{s}\left[f(x)\right] = \mathrm{sign}\left[f(x)\right]$ for conciseness. Hence, the partial derivative of $f_{T,i,j}$ with respect to $c_k^{(u_*)(n)}$ is given by

$$\frac{\partial f_{T,i,j}}{\partial c_k^{(u_*)}} = \frac{\partial f_{T,i,j}}{\partial c_k^{(u_*)}}|_1 + \frac{\partial f_{T,i,j}}{\partial c_k^{(u_*)}}|_2 + \frac{\partial f_{T,i,j}}{\partial c_k^{(u_*)}}|_3 + \frac{\partial f_{T,i,j}}{\partial c_k^{(u_*)}}|_4, \tag{C23}$$

where

$$\frac{\partial f_{T,i,j}}{\partial c_k^{(u_*)}}|_1 = -\frac{\Delta t}{r\cos\phi_j \Delta\lambda}\left(\frac{T_{i,j}}{2}\left(1+\mathrm{s}\left[u_{*,\mathrm{i+1/2,j}}\right]\right) + \frac{T_{i+1,j}}{2}\left(1-\mathrm{s}\left[u_{*,\mathrm{i+1/2,j}}\right]\right)\right)\lambda_{c,\mathrm{i+1/2}}^{a_k}\phi_{c,j}^{b_k}, \tag{C24a}$$

$$\frac{\partial f_{T,i,j}}{\partial c_k^{(u_*)}}|_2 = \frac{\Delta t}{r\cos\phi_j \Delta\lambda}\left(\frac{T_{i-1,j}}{2}\left(1+\mathrm{s}\left[u_{*,\mathrm{i-1/2,j}}\right]\right) + \frac{T_{i,j}}{2}\left(1-\mathrm{s}\left[u_{*,\mathrm{i-1/2,j}}\right]\right)\right)\lambda_{c,\mathrm{i-1/2}}^{a_k}\phi_{c,j}^{b_k}, \tag{C24b}$$

$$\frac{\partial f_{T,i,j}}{\partial c_k^{(u_*)}}|_3 = \frac{\Delta t}{r\cos\phi_j \Delta\lambda} T_{i,j}\left(\lambda_{c,\mathrm{i+1/2}}^{a_k} - \lambda_{c,\mathrm{i-1/2}}^{a_k}\right)\phi_{c,j}^{b_k}, \tag{C24c}$$

$$\frac{\partial f_{T,i,j}}{\partial c_k^{(u_*)}}|_4 = \frac{\Delta t}{r\cos\phi_j \Delta\lambda}\frac{T_{I,i,j}-T_{i,j}}{h_{i,j}}\left(\bar{h}_{\mathrm{i+1/2,j}}\lambda_{c,\mathrm{i+1/2}}^{a_k} - \bar{h}_{\mathrm{i-1/2,j}}\lambda_{c,\mathrm{i-1/2}}^{a_k}\right)\phi_{c,j}^{b_k}, \tag{C24d}$$

and the partial derivative of $f_{T,i,j}$ with respect to $c_k^{(v_*)(n)}$ is given by

$$\frac{\partial f_{T,i,j}}{\partial c_k^{(v_*)}} = \frac{\partial f_{T,i,j}}{\partial c_k^{(v_*)}}|_1 + \frac{\partial f_{T,i,j}}{\partial c_k^{(v_*)}}|_2 + \frac{\partial f_{T,i,j}}{\partial c_k^{(v_*)}}|_3 + \frac{\partial f_{T,i,j}}{\partial c_k^{(v_*)}}|_4, \tag{C25}$$

where

$$\frac{\partial f_{T,i,j}}{\partial c_k^{(v_*)}}|_1 = -\frac{\Delta t}{r\Delta\phi}\left(\frac{T_{i,j}}{2}\left(1+\mathrm{s}\left[v_{*,\mathrm{i,j+1/2}}\right]\right) + \frac{T_{i,j+1}}{2}\left(1-\mathrm{s}\left[v_{*,\mathrm{i,j+1/2}}\right]\right)\right)\lambda_{c,i}^{a_k}\phi_{c,\mathrm{j+1/2}}^{b_k}, \tag{C26a}$$

$$\frac{\partial f_{T,i,j}}{\partial c_k^{(v_*)}}|_2 = \frac{\Delta t}{r\Delta\phi}\left(\frac{T_{i,j-1}}{2}\left(1+\mathrm{s}\left[v_{*,\mathrm{i,j-1/2}}\right]\right) + \frac{T_{i,j}}{2}\left(1-\mathrm{s}\left[v_{*,\mathrm{i,j-1/2}}\right]\right)\right)\lambda_{c,i}^{a_k}\phi_{c,\mathrm{j-1/2}}^{b_k}, \tag{C26b}$$

$$\frac{\partial f_{T,i,j}}{\partial c_k^{(v_*)}}|_3 = \frac{\Delta t}{r\Delta\phi} T_{i,j}\left(\phi_{c,\mathrm{j+1/2}}^{b_k} - \phi_{c,\mathrm{j-1/2}}^{b_k}\right)\lambda_{c,i}^{a_k}, \tag{C26c}$$

$$\frac{\partial f_{T,i,j}}{\partial c_k^{(v_*)}}|_4 = \frac{\Delta t}{r\Delta\sin\phi}\frac{T_{I,i,j}-T_{i,j}}{h_{i,j}}\left(\left[\bar{h}_{\mathrm{i,j+1/2}}\cos\phi_{\mathrm{j+1/2}}\right]\phi_{c,\mathrm{j+1/2}}^{b_k} - \left[\bar{h}_{\mathrm{i,j-1/2}}\cos\phi_{\mathrm{j-1/2}}\right]\phi_{c,\mathrm{j-1/2}}^{b_k}\right)\lambda_{c,i}^{a_k}. \tag{C26d}$$

Derivatives of ML temperature equation at boundary points

The difference equation for ML temperature at boundary point (i,j) is written as (28)

$$T_{i,j}^{n+1} = T_{i,j}^{n} + \Delta t\frac{w_A}{h_{i,j}}\left(T_{A,i,j}^{n} - T_{i,j}^{n}\right), \tag{C27}$$

or

$$T_{i,j}^{n+1} = f_{T,B,i,j}\left(T_{1,1}, \cdots, c_1^{(T_A)}, \cdots, c_1^{(T_I)}, \cdots, c_1^{(h)}, \cdots, c_1^{(\bar{u}_*)}, \cdots, c_1^{(\bar{v}_*)}, \cdots\right), \tag{C28}$$

where the arguments of the function $f_{T,B,i,j}$, all implicitly defined at time level n, are the state variables defined in (31). The partial derivatives of $f_{T,B,i,j}$ that do not vanish are (superscript n omitted):

$$\frac{\partial f_{T,B,i,j}}{\partial T_{i,j}} = 1 - \Delta t \frac{w_A}{h_{i,j}}, \tag{C29}$$

$$\frac{\partial f_{T,B,i,j}}{\partial c_k^{(T_A)}} = \Delta t \frac{w_A}{h_{i,j}} \lambda_{c,i}^{a_k} \phi_{c,j}^{b_k}, \tag{C30}$$

$$\frac{\partial f_{T,B,i,j}}{\partial c_k^{(h)}} = -\Delta t \frac{w_A}{h_{i,j}^2} \left(T_{A,i,i} - T_{i,j}\right) \lambda_{c,i}^{a_k} \phi_{c,j}^{b_k}. \tag{C31}$$

Derivatives of the equations for the polynomial coefficients

The difference equation (30) is re-written as

$$c_k^{(\cdot)(n+1)} = f_{c_k^{(\cdot)}}\left(T_{1,1}, \cdots, c_1^{(T_A)}, \cdots, c_1^{(T_I)}, \cdots, c_1^{(h)}, \cdots, c_1^{(\bar{u}_*)}, \cdots, c_1^{(\bar{v}_*)}, \cdots\right), \tag{C32}$$

where the arguments of the function $f_{c_k^{(\cdot)}}$, all implicitly defined at time level n, are the state variables defined in (31). The partial derivatives of $f_{c_k^{(\cdot)}}$ that do not vanish are:

$$\frac{\partial f_{c_k^{(T_A)}}}{\partial c_k^{(T_A)}} = 1, \tag{C33a}$$

$$\frac{\partial f_{c_k^{(T_I)}}}{\partial c_k^{(T_I)}} = 1, \tag{C33b}$$

$$\frac{\partial f_{c_k^{(u_*)}}}{\partial c_k^{(u_*)}} = 1, \tag{C33c}$$

$$\frac{\partial f_{c_k^{(v_*)}}}{\partial c_k^{(v_*)}} = 1. \tag{C33d}$$

9 References

References

Anderson, B. D. O., and G. B. Moore. *Optimal filtering.* Englewood Cliffs, NJ, Prentice Hall, 1979.

Arhan, M., A. Colin de Verdière, and H. Mercier, Direct observations of the mean circulation at 48°N in the Atlantic Ocean, *J. Phys. Oceanogr.*, *19*, 161–181, 1989.

Bard, E., M. Arnold, P. Maurice, J. Duprat, J. Moyes, and J.-C. Duplessy, Retreat velocity of the North Atlantic polar front during the last deglaciation determined by ^{14}C accelerator mass spectrometry, *Nature*, *328*, 791–794, 1987.

Brogan, W. L. *Modern control theory.* Prentice Hall, Englewood Cliffs, New Jersey, 1991. 653 pp.

Bryson, A. E., and Y.-C. Ho. *Applied optimal control.* Taylor and Francis, 1975.

Chen, L. G., Mixed layer density ratio from the Levitus data, *J. Phys. Oceanogr.*, *25*, 691–701, 1995.

Colin de Verdière, A., H. Mercier, and M. Arhan, Mesoscale variability transition from the Western to the Eastern Atlantic along 48°N, *J. Phys. Oceanogr.*, *19*, 1149–1170, 1989.

Cushman-Roisin, B., Effects of horizontal advection on upper ocean mixing: A case of frontogenesis, *J. Phys. Oceanogr.*, *11*, 1345–1356, 1981.

de Ruijter, W. P. M., Effects of velocity shear in advective mixed-layer models, *J. Phys. Oceanogr.*, *13*, 1589–1599, 1983a.

de Ruijter, W. P. M., Frontogenesis in an advective mixed-layer model, *J. Phys. Oceanogr.*, *13*, 487–495, 1983b.

de Szoeke, R. A., On the effects of horizontal variability of wind stress on the dynamics of the ocean mixed layer, *J. Phys. Oceanogr.*, *10*, 1439–1454, 1980.

Deser, C., M. A. Alexander, S.-P. Xie, and A. S. Phillips, Sea surface temperature variability, *Annu. Rev. Marine Sci.*, *2*, 115–143, 2010.

Duplessy, J.-C., L. Labeyrie, M. Arnold, M. Paterne, J. Duprat, and T. C. E. Van Weering, Changes in surface salinity of the North Atlantic Ocean during the last deglaciation, *Nature*, *358*, 485–488, 1992.

Edwards, C. A., A. M. Moore, I. Hoteit, and B. D. Cornuelle, Regional ocean data assimilation, *Annu. Rev. Marine Sci.*, *7*, 21–42, 2015.

Fraser, D. C., 1967. *A new technique for the optimal smoothing of data*. Ph. D. thesis, Massachusetts Institute of Technology.

Fratantoni, D., North Atlantic surface circulation during the 1990's observed with satellite-tracked drifters, *J. Geophys. Res.*, *22,067-22,093*, 2001.

Gaspar, P., Modelling the seasonal cycle of the upper ocean, *J. Phys. Oceanogr.*, *18*, 161–180, 1988.

Gaspar, P., and C. Wunsch, Estimates from altimetric data of barotropic waves in the northwestern Atlantic Ocean, *J. Phys. Oceanogr.*, *19*, 1821–1844, 1989.

Gelb, A., J. F. Kasper, R. A. Nash, C. F. Price, and A. A. Sutherland. *Applied Optimal Estimation*. Technical Staff, The Analytic Sciences Corporation, M.I.T. Press, 1974.

Gill, A. E., and P. P. Niiler, The theory of the seasonal variability in the ocean, *Deep Sea Res.*, *20*, 141–177, 1973.

Haney, R. L., Surface thermal boundary conditions for ocean general circulation models, *J. Phys. Oceanogr.*, *1*, 241–248, 1971.

Johnston, T. M. S., and D. L. Rudnick, Observations of the transition layer, *J. Phys. Oceanogr.*, *39*, 780–797, 2009.

Kraus, E. B., and J. S. Turner, A one-dimensional model of the seasonal thermocline, *Tellus*, *19*, 98–105, 1967.

Labeyrie, L., H. Leclaire, C. Waelbroeck, E. Cortijo, J.-C. Duplessy, L. Vidal, M. Elliot, B. LeCoat, and G. Auffret. Temporal variability of the surface and deep waters of the North West Atlantic Ocean at orbital and millennial scales, R. Webb, P. U. Clark, and L. D. Keigwin (Eds.), *Mechanisms of Global Climate Change at Millennial Time Scales*, Volume 112 of *Geophysical Monograph*, pp. 77–98. Am. Geophys. Union, 1999.

Liebelt, P. B. *An introduction to optimal estimation.* Addison-Wesley, Reading, MA, 1967. 273 pp.

Mann, C. R., The termination of the Gulf Stream and the beginning of the North Atlantic Current, *Deep Sea Res.*, *14*, 337–359, 1967.

Marchesiello, P., J. C. McWilliams, and A. Shchepetkin, Open boundary conditions for long-term integration of regional oceanic models, *Ocean Modelling*, *3*, 1–20, 2001.

Martin, P. J., Simulation of the mixed layer at OWS November and Papa with several models, *J. Geophys. Res.*, *90*, 903–916, 1985.

Mehra, R. K., On the identification of variances and adaptive Kalman filtering, *IEEE Trans. Automat. Contr.*, *AC-15*, 175–184, 1970.

Monterey, G., and S. Levitus, Washington, D.C.: NOAA Atlas NESDIS 14, U.S. Gov. Printing Office, 1997.

Niiler, P. P., and E. B. Krauss. One-dimensional models of the upper ocean, E. B. Kraus edited by , *Modelling and prediction of the upper layers of the ocean*, pp. 143–172. Pergamon Press, Oxford, 1977.

Pedlosky, J. *Ocean Circulation Theory.* Springer, 1996. 453 pp.

Press, W. H., S. A. Teukolsky, W. T. Vetterling, and B. P. Flannery (Eds.). *Numerical Recipes (in Fortran) - The Art of Scientific Computing*, Volume Second edition. Cambridge University Press, 1992. 963 pp.

Price, J. F., R. A. Weller, and R. Pinkel, Diurnal cycling: Observations and models of the upper ocean response to diurnal heating, cooling, and wind mixing, *J. Geophys. Res.*, *91*, 8411–8427, 1986.

Rauch, H. E., F. Tung, and C. T. Striebel, Maximum likelihood estimates of linear dynamic systems, *AIAA J.*, *3*, 1445–1450, 1965.

Read, J. F., R. T. Pollard, P. I. Miller, and A. C. Dale, Circulation and variability of the North Atlantic Current in the vicinity of the Mid-Atlantic Ridge, *Deep Sea Res. I*, *57*, 307–318, 2010.

Risien, C. M., and D. B. Chelton, A global climatology of surface wind and wind stress fields from eight years of QuickSCAT scatterometer data, *J. Phys. Oceanogr.*, *38*, 2379–2413, 2008.

Rossby, H. T., The North Atlantic Current and surrounding waters: At the crossroads, *Rev. Geophys.*, *34*, 463–481, 1996.

Rudnick, D. L., and R. E. Davis, Frontogenesis in mixed layers, *J. Phys. Oceanogr.*, *18*, 434–457, 1988.

Rudnick, D. L., and R. A. Weller, The heat budget in the North Atlantic subtropical frontal zone, *J. Geophys. Res.*, *98*, 6883–6893, 1993.

Stengel, R. F. *Stochastic optimal control*. John Wilet & Sons, New York, 1986. 638 pp.

Stevens, D. P., On open boundary conditions for three dimensional primitive equation ocean circulation models, *Geophys. Astrophys. Fluid Dynamics*, *51*, 103–133, 1990.

Stommel, H. M., A conjectural regulating mechanism for determining the thermohaline structure of the ocean mixed layer, *J. Phys. Oceanogr.*, *23*, 142–150, 1993.

Stuiver, M., and P. J. Reimer, Extended C-14 data base and revised Calib 3.0 age calibration program, *Radiocarbon*, *35*, 215–230, 1993.

Stuiver, M., P. J. Reimer, E. Bard, W. Beck, G. S. Burr, K. A. Hughen, B. Kromer, G. McCormac, J. van der Plicht, and M. Spurk, Intcal98 radiocarbon age calibration, 24,000-0 cal B.P., *Radiocarbon*, *40*, 1041–1083, 1998.

Sun, O. M., S. R. Jayne, K. L. Polzin, B. A. Rather, and L. C. St. Laurent, Scaling turbulent dissipation in the transition layer, *J. Phys. Oceanogr.*, *43*, 2475–2489, 2013.

Waelbroeck, C., J.-C. Duplessy, E. Michel, L. Labeyrie, D. Paillard, and J. Duprat, The timing of the last deglaciation in North Atlantic climate records, *Nature*, *412*, 724–727, 2001.

Waelbroeck, C., L. Labeyrie, J.-C. Duplessy, J. Guiot, M. Labracherie, H. Leclaire, and J. Duprat, Improving past sea surface temperature estimates based on planktonic fossil faunas, *Paleoceanography*, *13*, 272–283, 1998.

Welander, P., Mixed layers and fronts in simple ocean circulation models, *J. Phys. Oceanogr.*, *11*, 148–152, 1981.

WOA, World Ocean Atlas, Washington, D.C.: U.S. Department of Commerce, 2013.

Wunsch, C. *Discrete inverse and state estimation problems*. Cambridge University Press, 2006. 371 pp.

10 Tables

10.1 Table 1: Parameters of the Ocean Mixed Layer Model

	definition	value	units
Ω	Earth angular velocity	7.3×10^{-5}	s^{-1}
r	Earth radius	6371	km
ρ_o	reference density	1025	kg m^{-3}
g	acceleration due to gravity	9.81	m s^{-2}
α	thermal expansion coefficient	2×10^{-4}	$°C^{-1}$
β	haline contraction coefficient	$0.8/\rho_o$	1
w_A	strength of air-sea heat exchange	9×10^{-6}	m s^{-1}

10.2 Table 2: Integral exponents of the polynomial approximations

	k									
	1	2	3	4	5	6	7	8	9	10
a_k	0	0	1	0	2	1	0	3	1	2
b_k	0	1	0	2	0	1	3	0	2	1

11 Figures

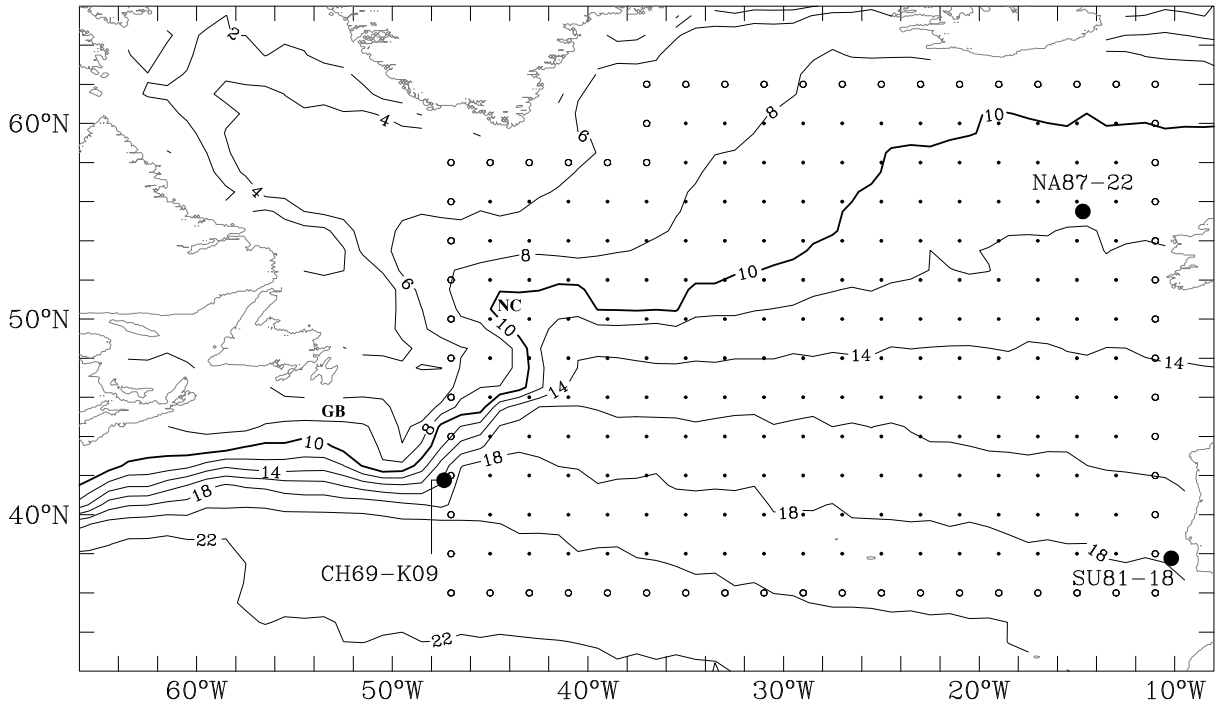

Figure 1: Map of the North Atlantic. The black lines are isopleths of modern annual mean SST (*WOA* (2013); contour interval of 2°C). The 10°C isotherm (thick line) traces approximately the Subpolar Front. The large black solid circles indicate the location of sediment cores considered in this study: SU81-18, CH69-K09, and NA87-22. The small solid and small open circles show, respectively, the interior and boundary points of the model grid. The Grand Banks (GB) and Northwest Corner (NC) are also located. Gray lines are coastlines.

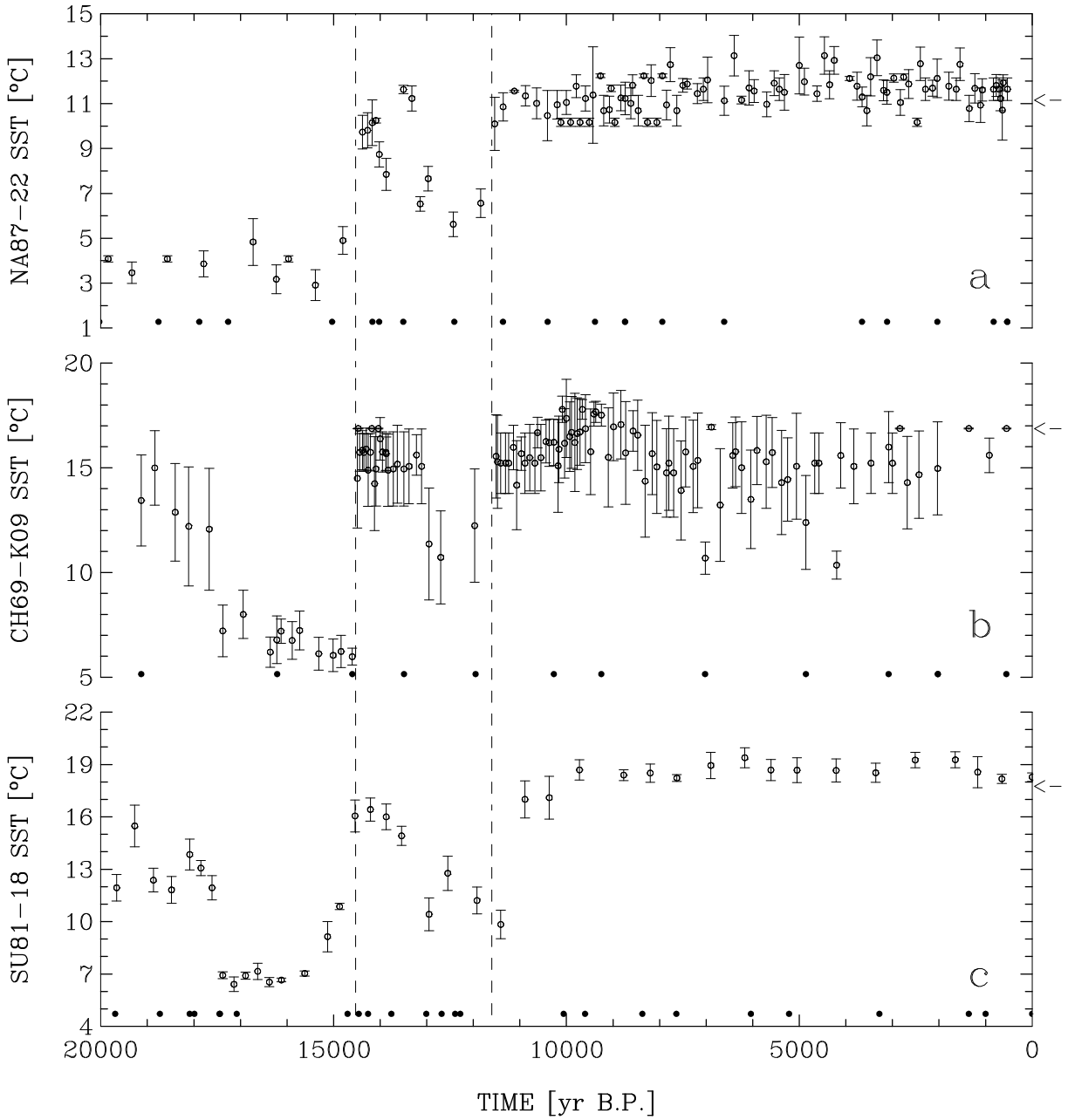

Figure 2: Records of SST for (a) core NA87-22, (b) core CH69-K09, and (c) core SU81-18. The open circles are the averages of the cold and warm season SSTs reconstructed from foraminiferal counts, and the vertical bars are their estimated errors. The solid circles at the bottom of each panel are the calendar ages for which planktonic foraminiferal ^{14}C dates are available. The vertical dashed lines show the two tie points used to construct the core chronologies in addition to the ^{14}C dates: the transition from Heinrich Event 1 to the Bølling (14.53 kyr BP) and the transition from the YD to the Holocene (11.60 kyr BP) (dates from *Waelbroeck et al.*, 2001). The arrow at the right of each panel shows the annual mean SST at the closest location in the World Ocean Atlas (*WOA*, 2013).

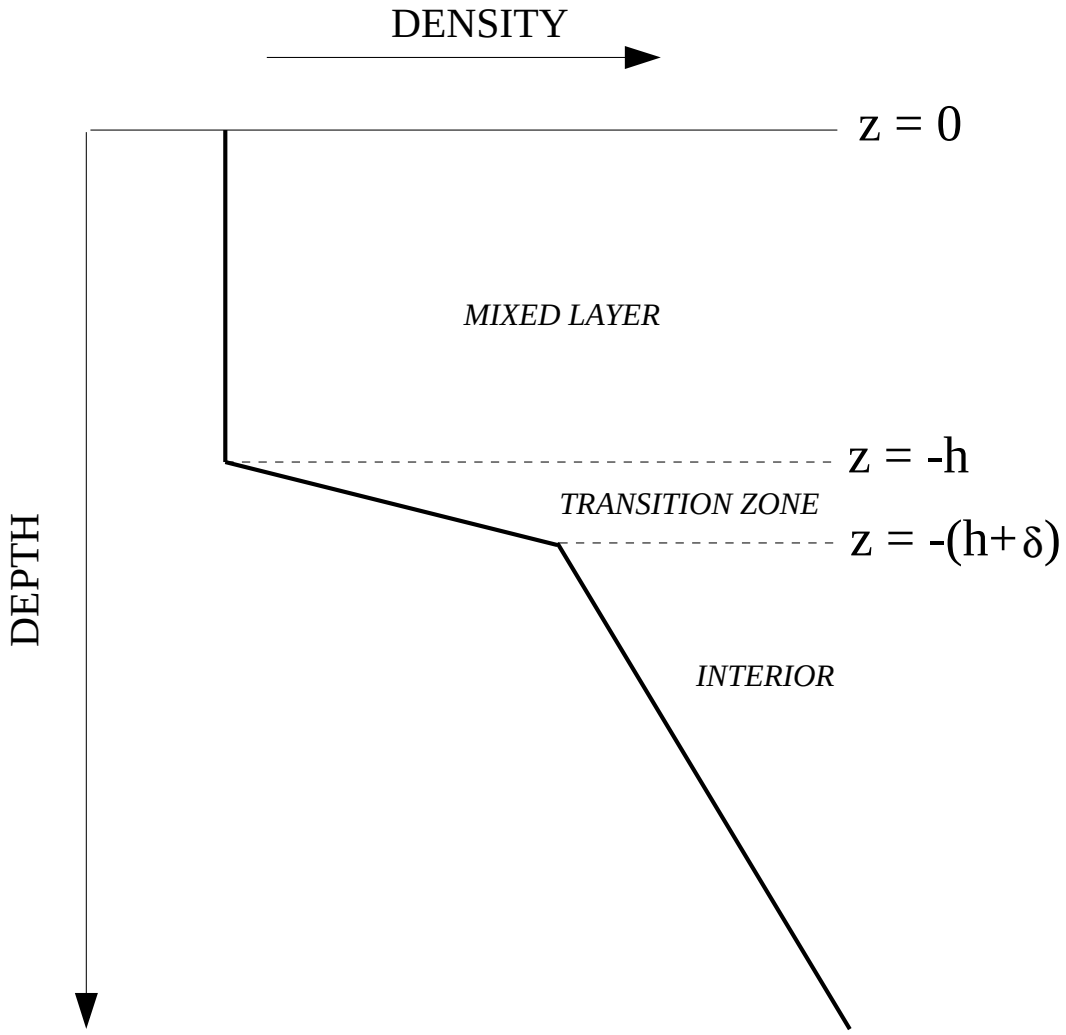

Figure 3: Schematic diagram of the ocean mixed-layer model.

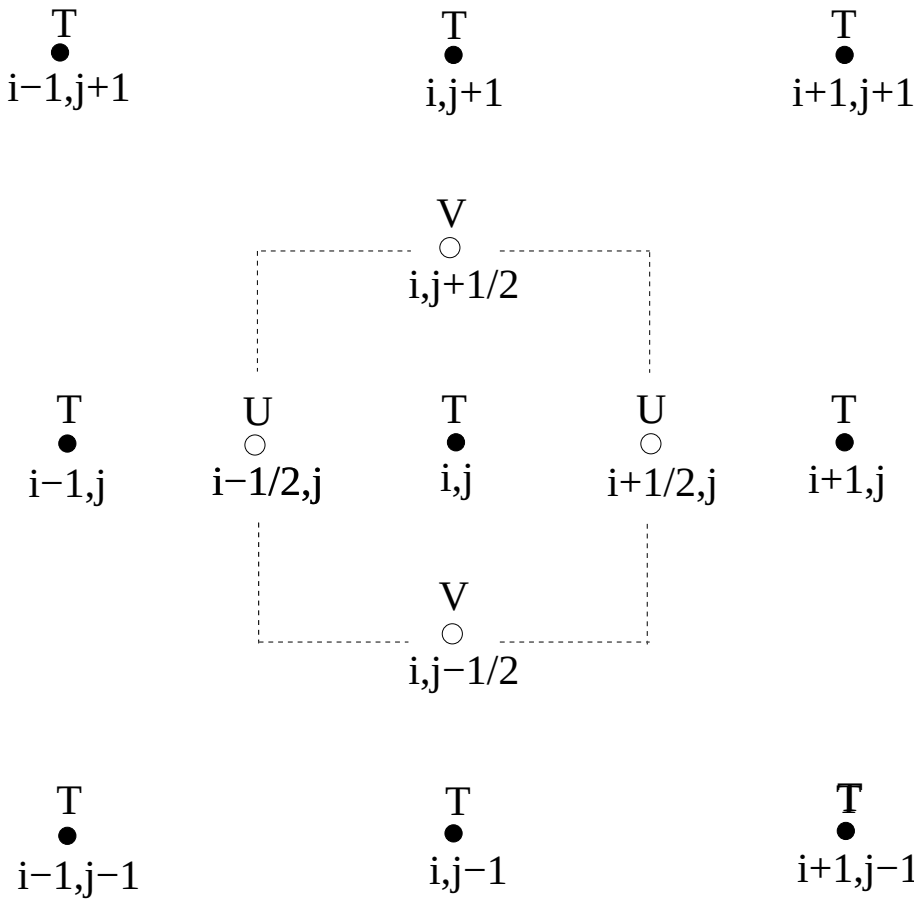

Figure 4: Staggered grid of the ocean mixed-layer model. The square bounded by dashed sides is the grid cell centered at the $T_{i,j}$-carrier point.

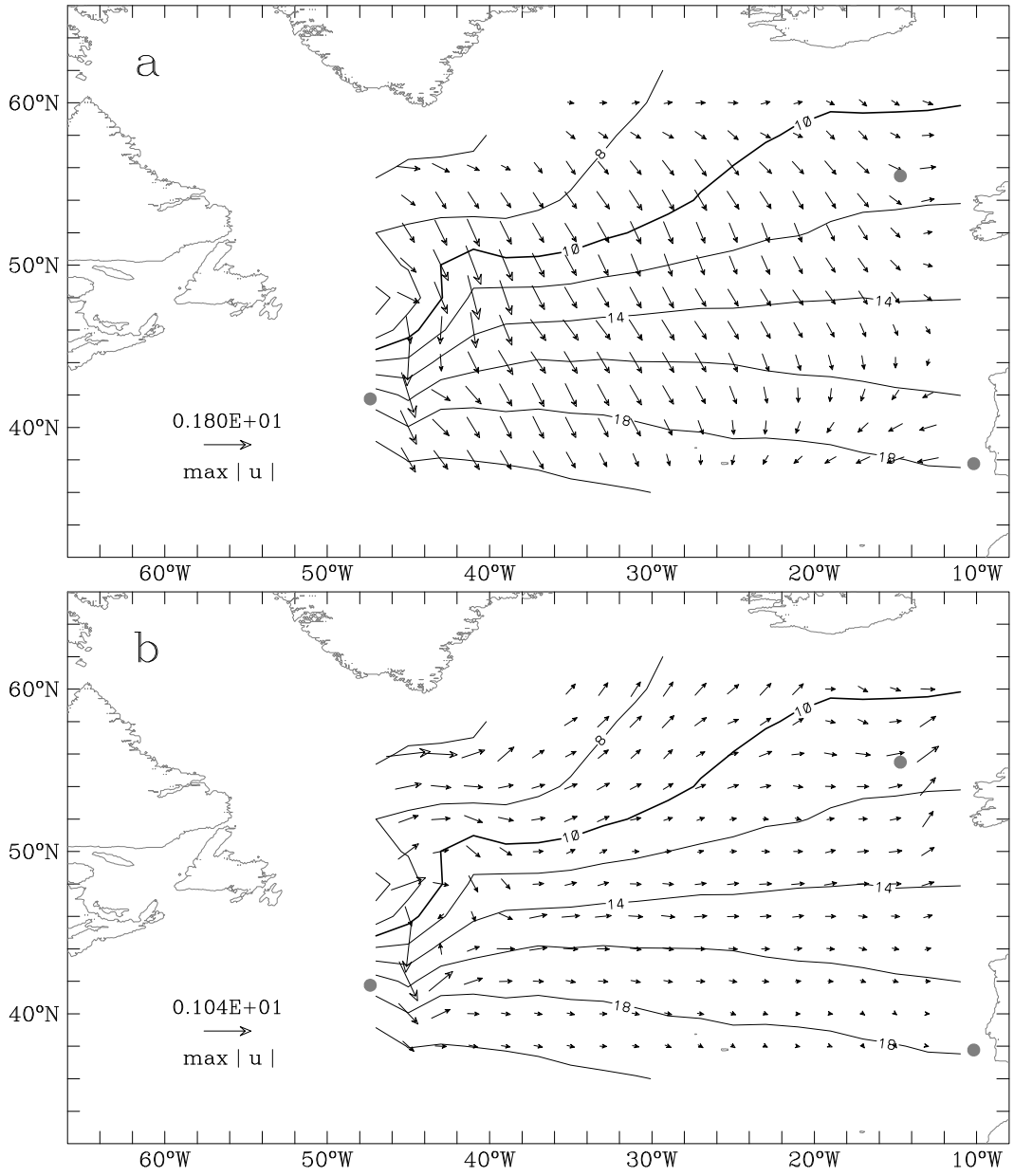

Figure 5: Distributions of ML temperature (contour interval of 2°C), ML total velocity $\bar{\mathbf{u}}_e+\bar{\mathbf{u}}_T+\bar{\mathbf{u}}_S$, and ML geostrophic velocity $\bar{\mathbf{u}}_T+\bar{\mathbf{u}}_S$ in the modern North Atlantic simulated by the model. The total and geostrophic velocities are shown in panel (a) and (b), respectively. The maximum amplitude in the velocity fields is 1.80 cm s^{-1} (a) and 1.04 cm s^{-1} (b). In both panels, the gray circles show the location of sediment cores SU81-18, CH69-K09, and NA87-22.

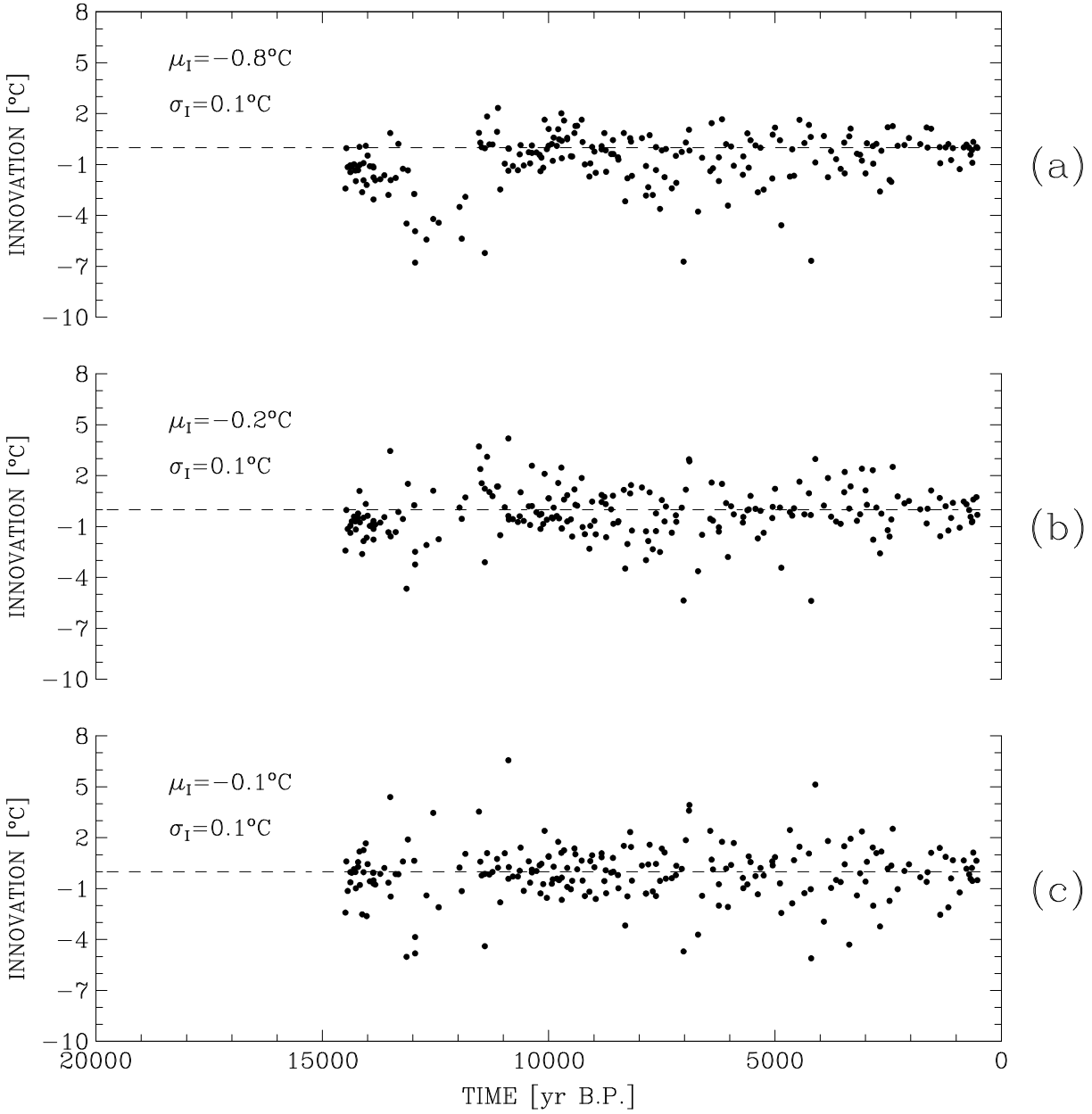

Figure 6: Time series of the elements of $\mathbf{z}_i - \mathbf{H}_i\hat{\mathbf{x}}_i(-)$ in three different LKF experiments with (a) $\epsilon = 10^{-4}$, (b) $\epsilon = 10^{-3}$, and (c) $\epsilon = 10^{-2}$. In each panel, μ_I and σ_I are, respectively, the average and the standard error of the innovation elements.

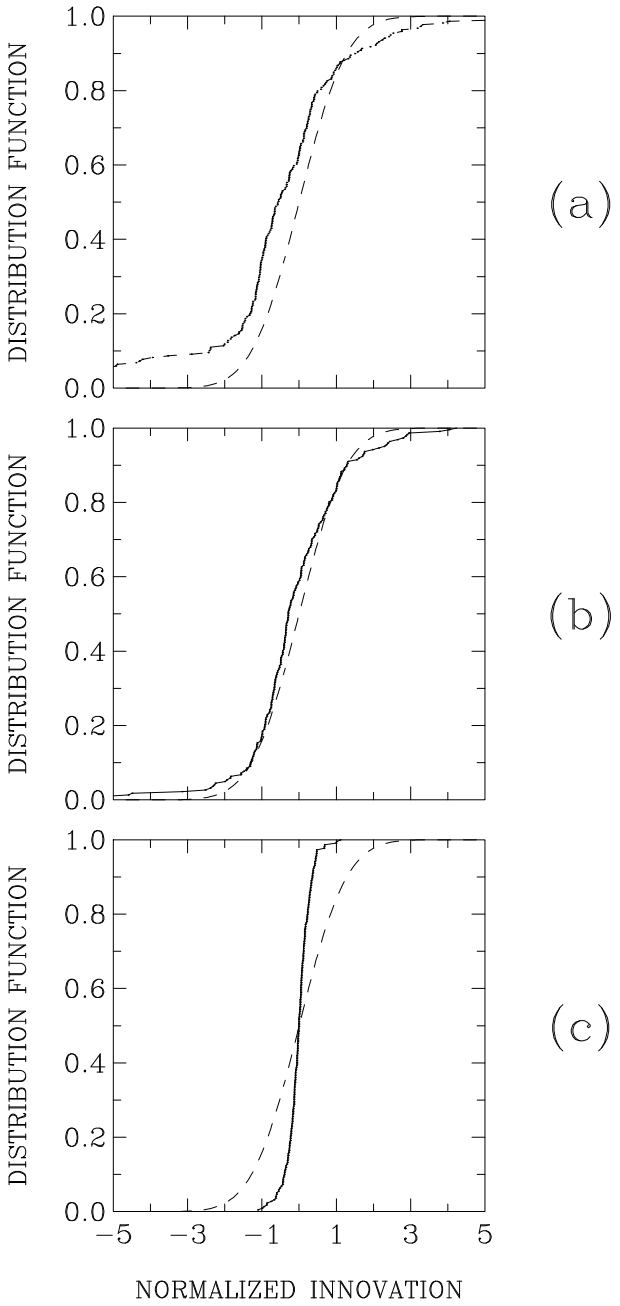

Figure 7: Distribution function of the elements of $\mathbf{z}_i - \mathbf{H}_i\hat{\mathbf{x}}_i(-)$ normalized to their standard deviations in three different LKF experiments with (a) $\epsilon = 10^{-4}$, (b) $\epsilon = 10^{-3}$, and (c) $\epsilon = 10^{-2}$. The dashed line in each panel is the normal distribution function with zero mean and unit variance.

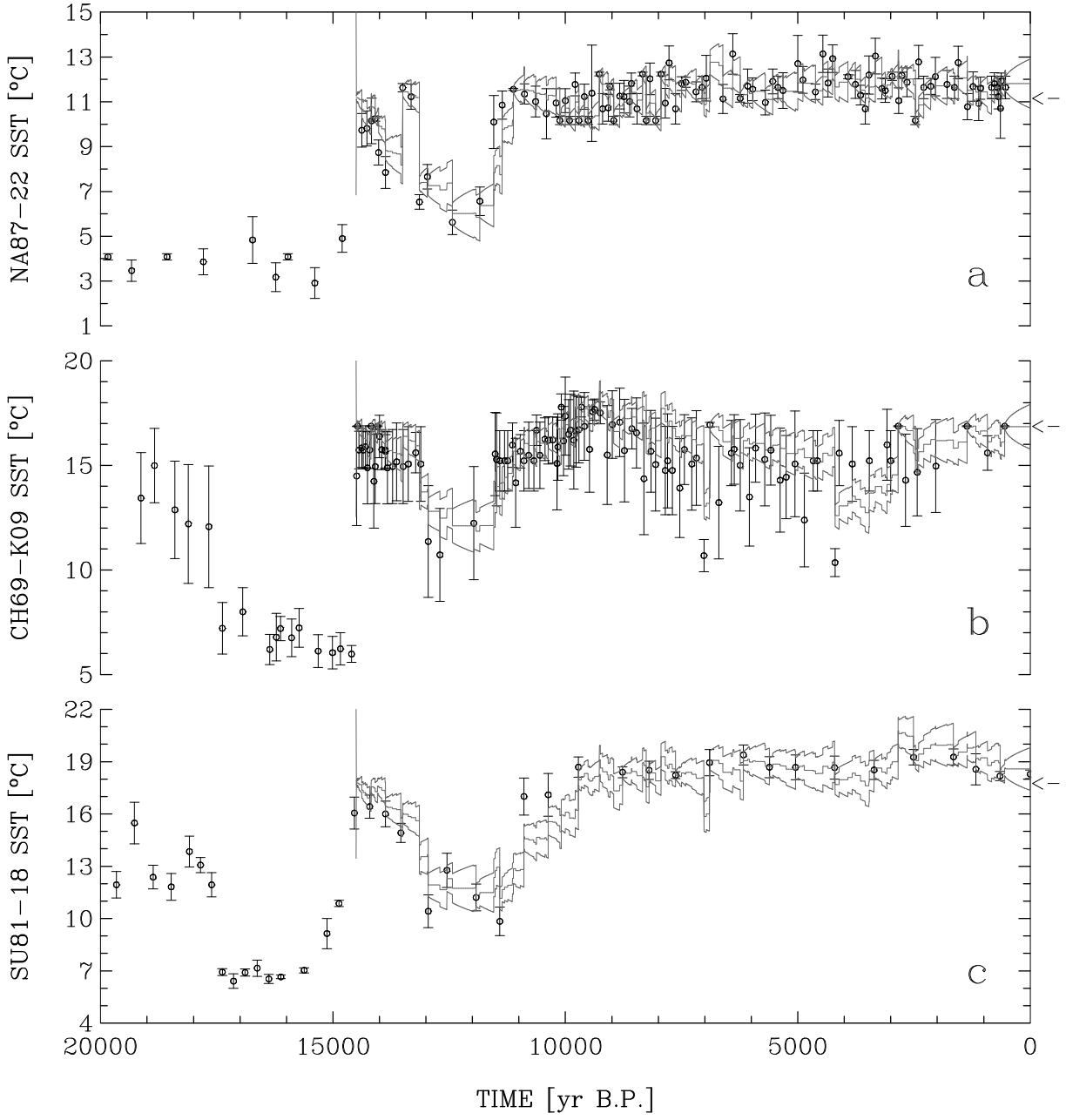

Figure 8: Reconstructed SSTs and filtered estimates of ML temperature for (a) core NA87-22, (b) core CH69-K09, and (c) core SU81-18. The open circles are the SSTs reconstructed from foraminiferal counts and the vertical bars are their estimated errors. The solid lines show the ML temperatures ($\pm$ one standard deviation) estimated from the LKF ($\epsilon = 10^{-3}$).

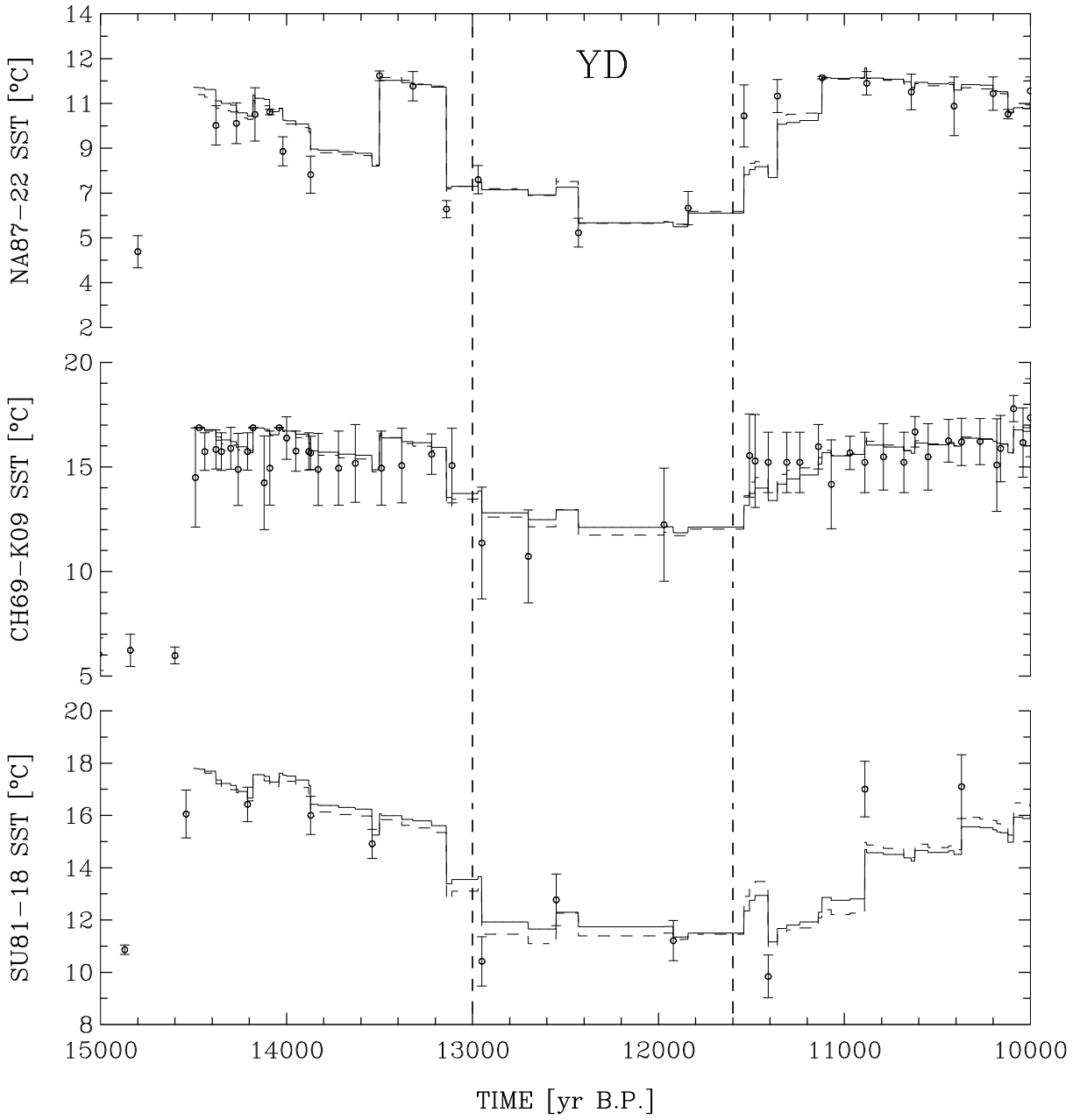

Figure 9: Reconstructed SSTs and filtered estimates of ML temperature for (a) core NA87-22, (b) core CH69-K09, and (c) core SU81-18. The open circles are the SSTs reconstructed from foraminiferal counts and the vertical bars are their estimated errors. The dashed lines show the temperatures estimated from the EKF and the solid lines show the temperatures estimated from the LKF. The vertical dashed lines show approximate dates of the onset (13 kyr BP) and termination (11.6 kyr BP) of the YD.

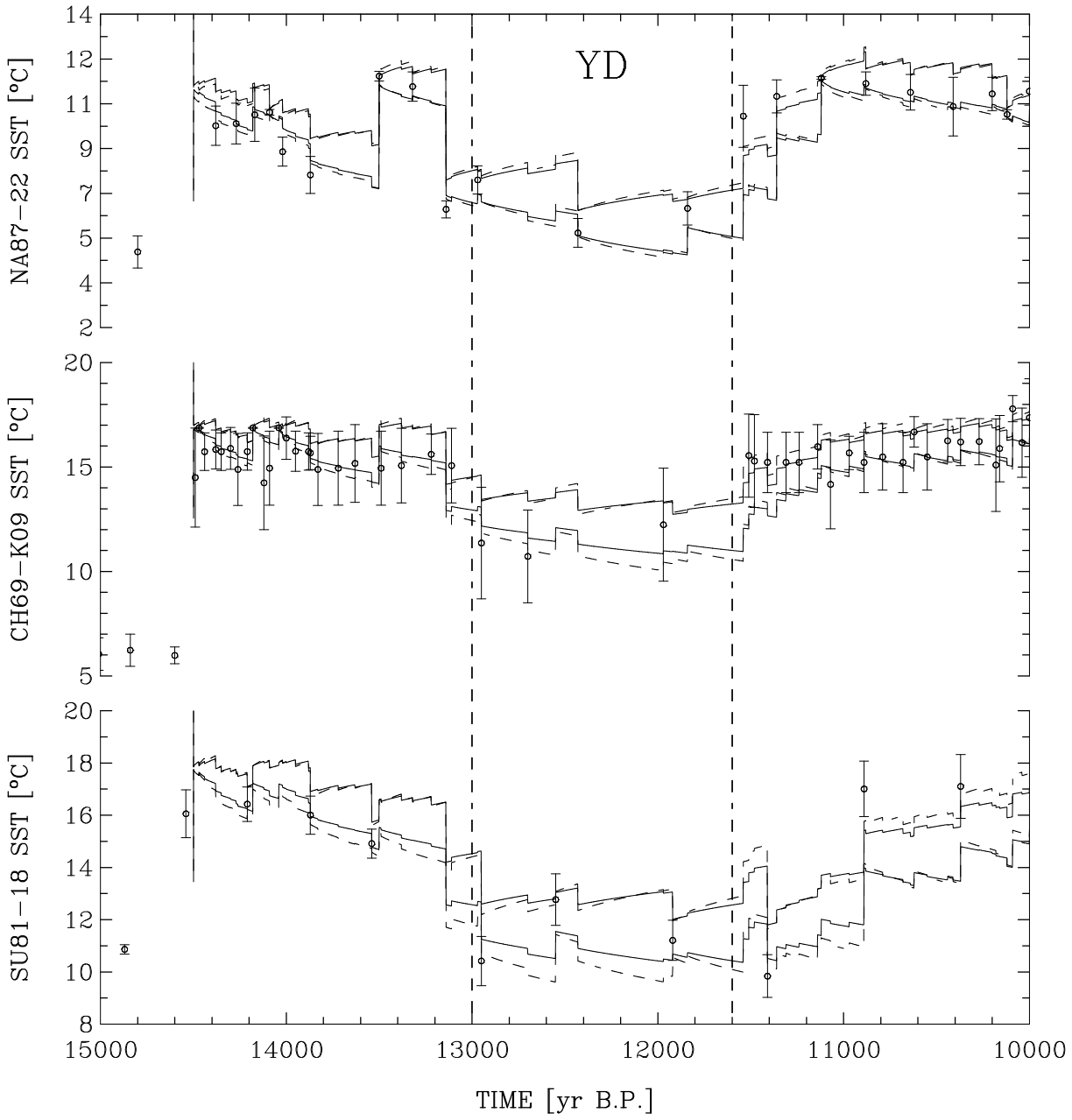

Figure 10: Reconstructed SSTs and filtered estimates of ML temperature for (a) core NA87-22, (b) core CH69-K09, and (c) core SU81-18. The open circles are the SSTs reconstructed from foraminiferal counts and the vertical bars are their estimated errors. The dashed lines show the temperatures ± one standard deviation estimated from the EKF and the solid lines show the ML temperatures ± one standard deviation estimated from the LKF. The vertical dashed lines show approximate dates of the onset (13 kyr BP) and termination (11.6 kyr BP) of the YD.

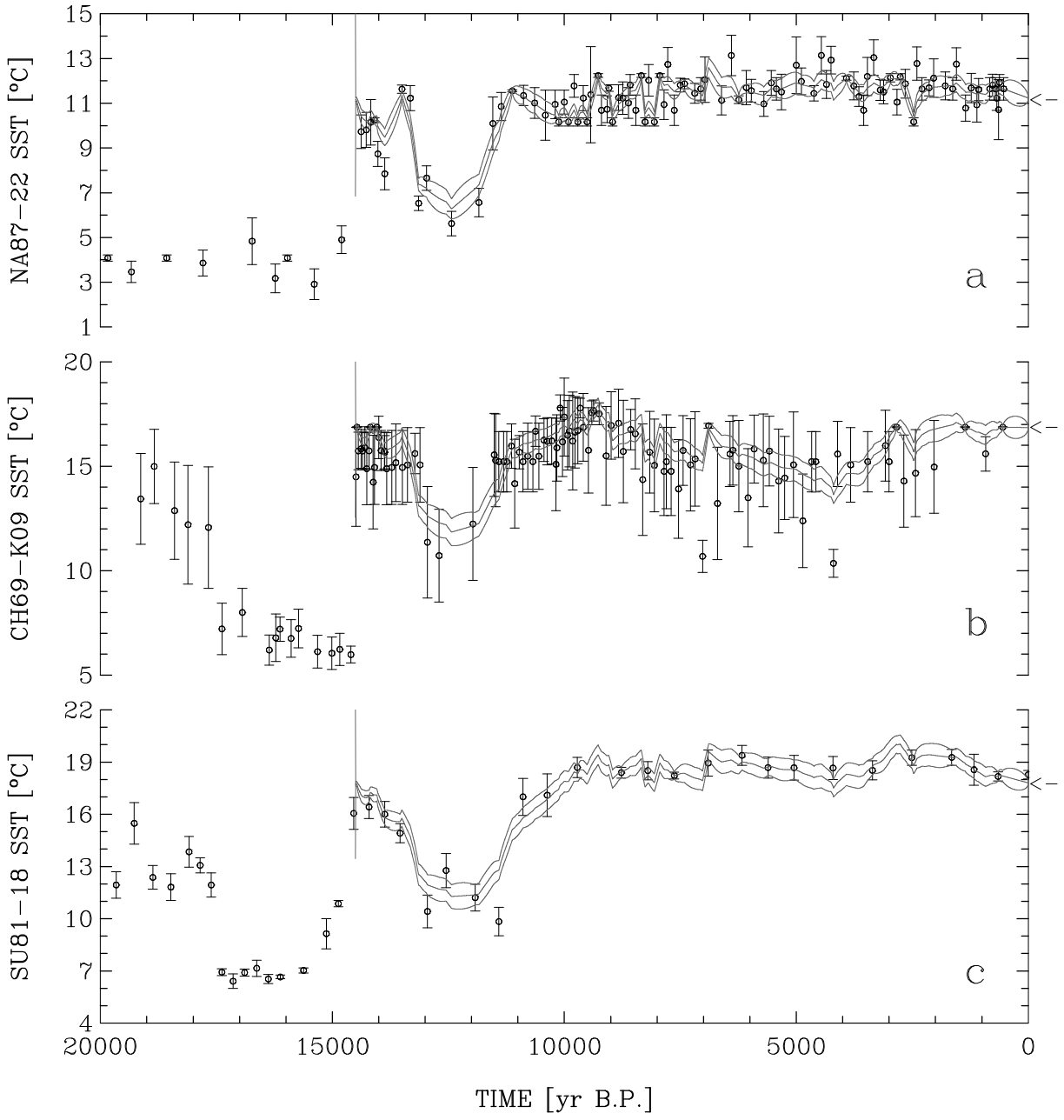

Figure 11: Reconstructed SSTs and smoothed estimates of ML temperature for (a) core NA87-22, (b) core CH69-K09, and (c) core SU81-18. The open circles are the SSTs reconstructed from foraminiferal counts and the vertical bars are their estimated errors. The solid lines show the ML temperatures (± one standard deviation) estimated from the linearized smoother.

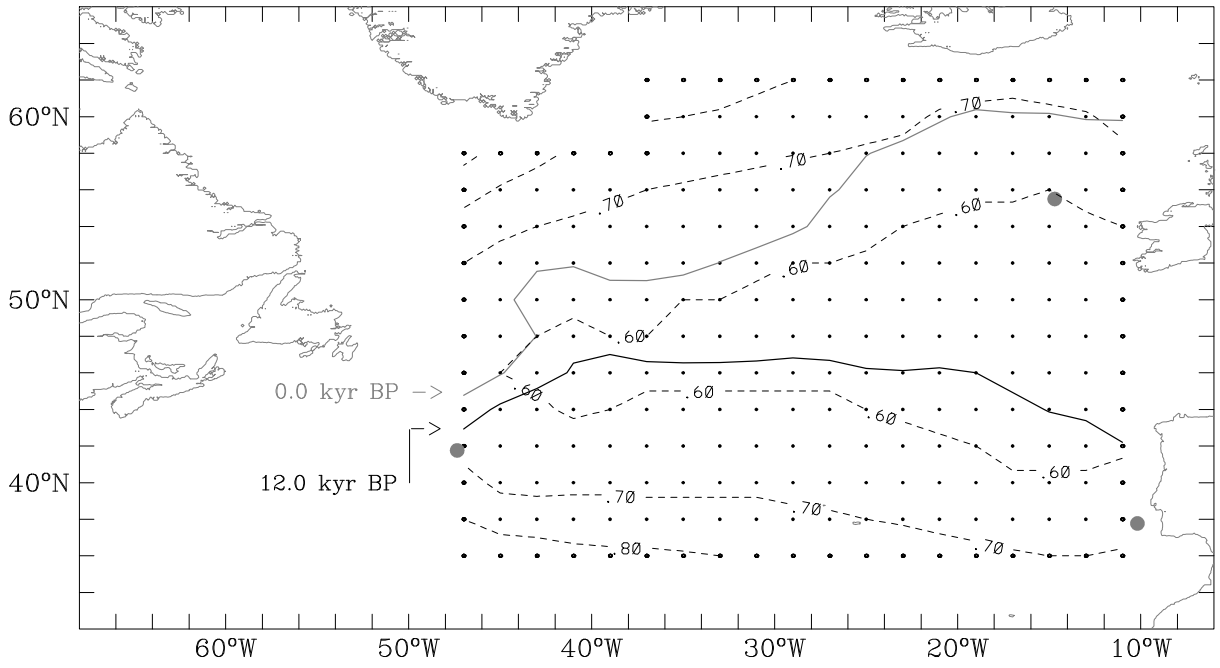

Figure 12: Position of the 10°C ML isotherm at 0 yr BP (solid gray line) and 12,000 yr BP (solid black line) and distribution of ML temperature error at 12,000 yr BP (dashed black lines; contour interval of 0.1°C) in the smoothing solution. The gray circles show the location of sediment cores SU81-18, CH69-K09, and NA87-22. The small solid and small open circles are, respectively, the interior and boundary points of the model grid.